ELSEVIER

Contents lists available at ScienceDirect

Atmospheric Environment

journal homepage: www.elsevier.com/locate/atmosenv



Rapid formation of molecular bromine from deliquesced NaBr aerosol in the presence of ozone and UV light



Paul Nissenson ^a, Lisa M. Wingen ^b, Sherri W. Hunt ^c, Barbara J. Finlayson-Pitts ^{b,*}, Donald Dabdub ^{d,*}

- ^a California State Polytechnic University, Pomona, Department of Mechanical Engineering, Pomona, CA 91768-4062, USA
- ^b University of California, Irvine, Department of Chemistry, Irvine, CA 92697-2025, USA
- ^c National Center for Environmental Research, United States Environmental Protection Agency, Washington, DC 20460-0001, USA
- ^d University of California, Irvine, Department of Mechanical and Aerospace Engineering, Irvine, CA 92697-3975, USA

HIGHLIGHTS

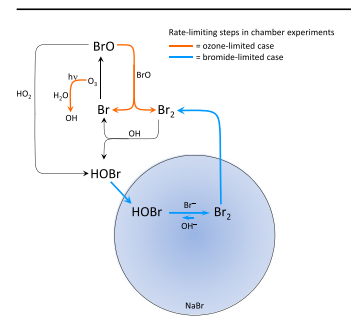
- Br₂ is produced rapidly from liquid NaBr aerosols in the presence of O₃ and UV light.
- The Br₂ production mechanism is determined through multi-phase kinetics modeling.
- The mechanism involves gas- and aqueous-phase chemistry, as well as mass transport.
- Rate-limiting steps vary in time and depend on the initial levels of O₃ and bromide.

ARTICLE INFO

Article history:
Received 21 June 2013
Received in revised form
31 January 2014
Accepted 24 February 2014
Available online 25 February 2014

Keywords: Bromide oxidation Sensitivity analysis Sea-salt aerosol Aerosol modeling Interface chemistry

G R A P H I C A L A B S T R A C T



ABSTRACT

The formation of gas-phase bromine from aqueous sodium bromide aerosols is investigated through a combination of chamber experiments and chemical kinetics modeling. Experiments show that $Br_{2(g)}$ is produced rapidly from deliquesced NaBr aerosols in the presence of OH radicals produced by ozone irradiated by UV light. The mechanisms responsible for the "bromine explosion" are examined using a comprehensive chemical kinetics Model of Aqueous, Gaseous, and Interfacial Chemistry (MAGIC). A sensitivity analysis on the model confirms that a complex mechanism involving gas-phase chemistry, aqueous-phase chemistry, and mass transfer is responsible for most of the observed bromine. However, the rate-limiting steps in the bromine explosion pathway vary, depending on the availability of ozone and bromide in the system. Interface reactions, an important source of bromine production under dark conditions, account for only a small fraction of total bromine under irradiation. Simulations performed with gaseous ozone and aerosol bromide concentrations typical of the marine boundary layer also show $Br_{2(g)}$ production, with $BrO_{(g)}$ and $HOBr_{(g)}$ as the dominant Br-containing products through this mechanism. Aerosol bromide is depleted after several hours of daylight, with photolysis of $BrO_{(g)}$ and $HOBr_{(g)}$ becoming major sources of Br atoms that continue generating $Br_{2(g)}$ after aerosol bromide is depleted.

1. Introduction

Bromine plays an important role in tropospheric ozone depletion events (ODEs) that have been observed at ground level in the polar spring (Barrie et al., 1988; Finlayson-Pitts et al., 1990; Fan and

^{*} Corresponding authors.

E-mail addresses: bjfinlay@uci.edu (B.J. Finlayson-Pitts), ddabdub@uci.edu
(D. Dabdub).

Jacob, 1992; Sander and Crutzen, 1996; Vogt et al., 1996; Barrie and Platt, 1997; Foster et al., 2001; Bottenheim et al., 2002; Spicer et al., 2002; Tarasick and Bottenheim, 2002; Sander et al., 2003; Simpson et al., 2007; Piot and von Glasow, 2008; Liao et al., 2012) and over salt lakes and dry lake beds (Hebestreit et al., 1999; Matveev et al., 2001: Stutz et al., 2002: Hönninger et al., 2004: Tas et al., 2006: Smovdzin and von Glasow, 2009). ODEs are often characterized by a rapid drop in the concentration of ozone and a simultaneous rise in concentration of reactive gas-phase bromine compounds, such as Br₂, BrO, and BrCl. Bromine chemistry is known to be key in the onset of ODEs in these regions and sea-salt, either on the snow pack or in particles, is believed to be the source of bromine. However, the exact mechanisms that convert bromide ions to gaseous bromine compounds are unclear (Simpson et al., 2007; Piot and von Glasow, 2008; Smoydzin and von Glasow, 2009; Abbatt et al., 2012; Pratt et al., 2013).

Less severe ODEs also occur in the marine boundary layer over mid-latitude oceans, particularly during sunrise (Dickerson et al., 1999; Nagao et al., 1999; Galbally et al., 2000). Halogens released from sea-salt aerosols, especially bromine, are thought to be the main cause of these smaller ODEs (Sander and Crutzen, 1996; Vogt et al., 1996). Sea-salt aerosols are the major source of inorganic bromine in the marine boundary layer, although other sources may be important locally (Sander et al., 2003).

Many laboratory studies have examined the release of gaseous bromine species from particles or solutions containing bromide (Finlayson-Pitts and Johnson, 1988; Finlayson-Pitts et al., 1990; Berko et al., 1991: Hirokawa et al., 1998: Oum et al., 1998a.b: Behnke et al., 1999: DeHaan et al., 1999: Anastasio and Mozurkewich, 2002: Hunt et al., 2004; Frinak and Abbatt, 2006; Clifford and Donaldson, 2007; George and Anastasio, 2007; Oldridge and Abbatt, 2011; Buxmann et al., 2012). Hirokawa et al. (1998) found that "almost deliquesced" NaBr particles placed on a glass filter produced Br_{2(g)} when exposed to both ozone and water vapor. Interestingly, no significant differences were observed in Br_{2(g)} production when a Xe arc lamp (with an optical filter to remove wavelengths <290 nm) illuminated the system, even though Br_{2(g)} readily photolyzes under actinic conditions (Finlayson-Pitts et al., 2000). Anastasio and Mozurkewich (2002) reported that $Br_{2(g)}$ formed when bromide was deposited onto a glass surface and exposed to ozone, and that the rate of Br2(g) formation is faster in the presence of UV light (254 nm) than in the dark. However, observed concentrations of Br_{2(g)} were orders of magnitude greater than expected based on known aqueous- and gas-phase chemistry. Recently, Zetzsch and coworkers reproduced the "bromine explosion" observed in the Arctic using an environmental chamber and dry NaCl/NaBr samples at sea water proportions, and showed that at high relative humidities (≥60%) the O₃ loss was greater than expected based on known halogen chemistry (Buxmann et al., 2012). Hunt et al. (2004) found that deliquesced NaBr aerosols in the dark produced $Br_{2(g)}$ in the presence of ozone. In that study, a two-phase kinetics Model of Aqueous, Gaseous, and Interfacial Chemistry (MAGIC) was utilized to examine the mechanisms of bromine formation. As in Anastasio and Mozurkewich (2002), known aqueous- and gas-phase chemistry significantly underpredicted observed $\text{Br}_{2(g)}$ concentrations. Hunt et al. (2004) reported that model predictions matched experimental measurements only when a heterogeneous reaction between gaseous ozone and bromide residing at the aerosol surface was included in MAGIC,

$$O_{3(g)} + Br_{(surf)}^{-} \rightarrow \frac{1}{2} Br_{2(g)} + O_{3(aq)}^{-}. \tag{1} \label{eq:1}$$

Molecular dynamics simulations by Jungwirth and Tobias (2002) and Hunt et al. (2004) showed that both bromide and

ozone can reside at the surface of deliquesced NaBr aerosols, allowing such a reaction to occur in the dark. Nissenson et al. (2009) probed the sensitivity and uncertainty from various individual steps that lead to Br₂ formation in the dark and for one limited set of conditions during irradiation.

In the presence of water vapor, photolysis of ozone produces hydroxyl radicals (Seinfeld and Pandis, 1998) that are known to oxidize bromide ions (Zehavi and Rabani, 1972). The present study extends the work by Hunt et al. (2004) by investigating how the production of OH affects bromine production from deliquesced NaBr aerosols. Previous studies have suggested that a reaction between $OH_{(g)}$ and chloride ions occurs at the surface of NaCl aerosols (Finlayson-Pitts et al., 2000; Knipping et al., 2000; Knipping and Dabdub, 2002; Laskin et al., 2006). Since bromide ions are more enhanced at the surface than chloride ions (Jungwirth and Tobias, 2001, 2002; Ghosal et al., 2005; Guzman et al., 2012) an analogous surface reaction between $OH_{(g)}$ and bromide seems likely,

$$OH_{(g)} + Br_{(surf)}^{-} \rightarrow \frac{1}{2} Br_{2(g)} + OH_{(aq)}^{-}. \tag{2} \label{eq:2}$$

Initial modeling studies by Thomas et al. (2006) and Nissenson et al. (2009) suggested that gaseous bromine production via reaction (2) is much slower than production due to aqueous-phase processes. However, these simulations were not benchmarked against specific experimental data under well-defined conditions. The purpose of the present study is to integrate the results of experiments with modeling in a quantitative manner in order to define the most important aspects of the chemical and physical mechanisms responsible for the observed "bromine explosion." This integrated modeling and experimental approach allows for the observation of changes in rate-limiting steps as a function of time as reactants are depleted, as well as examination of rate-limiting steps under different initial conditions.

In this study, deliquesced NaBr aerosols are exposed to ozone, water vapor, and UV light from low pressure mercury lamps (primarily 254 nm) to generate OH radicals. The total aerosol surface area and liquid volume is varied among experiments, changing the availability of bromide in the system. In all experiments, both BrO and Br₂ production increase rapidly upon photolysis. The MAGIC model is used to simulate four typical experiments with a wide range of initial conditions. There are three major improvements in the modeling methodology and analysis of modeling results compared to Nissenson et al. (2009): (1) The NaBr aerosol size distribution, initial concentration of chemical species, and photolysis rate constants used in the simulations for the current study are based on measurements from chamber experiments, while Nissenson et al. (2009) used hypothetical chamber conditions in their simulations; (2) In the current study, measured concentrations of Br_{2(g)}, BrO_(g), and $O_{3(g)}$ provide a check on the model results, while Nissenson et al. (2009) only attempted to achieve qualitative agreement between simulations and unpublished data from chamber experiments; (3) Lastly, the current study examines the time-dependence of ratelimiting steps in the bromine explosion mechanism and determines their contribution to model uncertainty during the entire illumination period, while Nissenson et al. (2009) only examined these quantities at the time of peak $Br_{2(g)}$ concentration.

Global sensitivity and uncertainty analyses are conducted on MAGIC to determine the important chemical and physical processes causing the observed bromine explosion and to identify the input parameters (e.g., chemical reaction rate constants, mass accommodation coefficients, etc.) that contribute the most uncertainty in the model output. Other studies have also used a combination of Monte Carlo sampling and linear regression techniques to gain insight into the production of important species from

chemical mechanisms (Derwent and Høv, 1988; Gao et al., 1995, 1996; Rodriguez and Dabdub, 2003; Nissenson et al., 2008, 2009). The sensitivity analysis presented here uses Latin Hypercube sampling, an efficient form of Monte Carlo sampling, to vary all input parameters over their full range of uncertainties (McKay et al., 1979). Multiple linear regression is used on the model output to identify the rate-limiting steps in $Br_{2(g)}$ formation from the NaBr aerosol. The sensitivity analysis also establishes uncertainty ranges for the model output that are compared with the observed $Br_{2(g)}$, $BrO_{(g)}$, and $O_{3(g)}$ concentrations. The results of the uncertainty analysis expose the parts of the bromine explosion mechanism that have the greatest impact on model performance and chemistry.

Finally, additional simulations are conducted using conditions similar to those found in the remote marine boundary layer in order to examine how the rate-limiting steps in $\text{Br}_{2(g)}$ production in the real atmosphere may differ from the rate-limiting steps in the experiments.

2. Methodology

2.1. Experimental

Aerosol experiments are conducted in a stainless steel and aluminum 561 L chamber described in detail elsewhere (DeHaan et al., 1999). Briefly, the top panels of the chamber hold quartz windows for photolysis using low pressure Hg lamps $(\lambda_{max} = 254 \text{ nm})$ and the chamber is evacuable to $<\!10^{-2}$ Torr using a dry pump (Busch, Cobra DS252). All experiments are initiated by adding air (Scott-Marrin, Riverside, CA; ultrapure, $NO_x < 0.001$ ppm, $SO_2 < 0.001$ ppm; THC < 0.01 ppm; CO < 0.01 ppm) to the chamber to pressures of 680-720 Torr and adjusting the relative humidity (RH) to 65-71% (Vaisala, HMP432) by passing some of the air through a water bubbler (Barnstead, $>18.0 \text{ M}\Omega$ cm). Polydisperse NaBr particles are added by flowing N₂ (Oxygen Services Co., 99.999%) through an atomizer (TSI, model 3076) containing a solution of 1% (w/w) NaBr (Alfa Products, Ultrapure) and then through a diffusion dryer into the chamber. A gaseous mixture of O₃ in O₂ is generated using an ozonizer (Polymetrics, model T-816) and a known volume is flushed in with dry air to a final pressure of ~765 Torr through a glass tube centered in the chamber that contains small holes to aid mixing. At that time the first dark period of the experiment begins, lasting 40-60 min before the UV lamps are turned on. After a UV period of ~ 10 min, the lamps are turned off and the second dark period of the experiment begins. The RH remains above the deliquescence point of NaBr (DRH = 58%) for the entire experiment to sustain the aqueous phase of the NaBr aerosols.

All inner metal surfaces are coated with halocarbon wax (Halocarbon Products Inc., Series 1500) to minimize wall reactivity. To remove salts and products from previous experiments, the chamber walls were cleaned frequently with Nanopure water. The frequency of cleaning needed was determined using the following procedure. NaBr particle experiments were alternated with control experiments in which only O_{3(g)} and humid air (no NaBr aerosol) were exposed to UV radiation. Br_{2(g)} measurements from several of these alternating experiments showed that wall reactions did not contribute significantly to gaseous Br2 until at least four NaBr particle experiments had been conducted without cleaning the chamber. Br_{2(g)} measured in control experiments was considered significant if it was >10% of the peak $Br_{2(g)}$ measured in a NaBr particle experiment. Of the four experimental cases presented here, three were carried out in a freshly cleaned chamber and the fourth case had only one NaBr aerosol experiment performed before it. Additional details regarding control experiments can be found in Supplementary Material.

The relative importance of OH loss to NaBr particles versus OH loss to the chamber walls is also compared by examining the total available surface area of the particles and walls, and the reaction probability of the particles and walls with OH. The surface area of the chamber walls is 4×10^4 cm², while the total particle surface area is 84-580 cm² for cases A-D (calculated using data from Table 1 and taking into account the 561 L chamber volume). Measurements of OH loss on halocarbon wax-coated surfaces have been reported in many studies (Burrows et al., 1984; Sridharan et al., 1984; Boodaghians et al., 1987; Hsu et al., 1987; Bertram et al., 2001), including from this laboratory (Ganske et al., 1991; Finlayson-Pitts et al., 1992; Ganske et al., 1992). In the fast flow discharge tube with a 1" inner diameter used in this laboratory, an average first order rate constant of 5 s⁻¹ was measured, which correlates to an uptake probability of $\gamma=2\times10^{-4}$ for OH on halocarbon wax. In comparison, the overall surface reaction probability for OH with NaBr aerosol particles in this study is $\gamma = 0.5$ (Supplementary Table 2). Taking into account the surface area of the particles and walls, as well as the reaction probability of OH with the particles and walls, the rate of OH loss to the particles is 5-35 times larger than the loss to the chamber walls for cases A–D based on laboratory measurements. As discussed in the Supplementary Material, this is an overestimate of the contribution from wall reactions because particle surfaces are more readily available to OH throughout most of the chamber volume.

In situ measurements of gas-phase species are conducted using two sets of White cell optics (White, 1942) located inside the chamber for collection of infrared and UV-visible spectra, both with total path lengths of 52.5 m. FTIR spectra (Mattson, Infinity 60AR) are collected continuously at 0.5 cm⁻¹ resolution to measure gaseous O₃ and CO₂. UV-visible spectra also are collected continuously using a high pressure Xe arc lamp light source (Oriel, 75 W, model 6263), a spectrometer (Jobin-Yvon, Spex, model HR460) with a holographic grating blazed at 330 nm with 1200 grooves mm⁻¹, and a 1024 channel photodiode array detector (Princeton Instruments, model PDA-1024). The UV-absorbing gases BrO and O₃ are detected and quantified in the range 290–330 nm using differential optical absorption spectroscopy (DOAS) techniques (Gomer et al., 1995; Stutz and Platt, 1996; Platt and Stutz, 1998).

Aerosol distributions are measured three or more times during the initial dark period and again at the end of the UV period using a scanning mobility particle sizer (SMPS; TSI, model 3071) with a condensation particle counter (CPC; TSI, model 3025A). Median electrical mobility aerosol diameters observed during the dark periods are in the range of 160-260 nm ($\sigma = 1.7-1.8$).

Gaseous Br₂ is measured using a dual quadrupole atmospheric pressure ionization mass spectrometer (API-MS, Perkin–Elmer Sciex, API 300) in negative ion mode. Specific detection of Br_{2(g)} is achieved by operating each quadrupole at a fixed mass, with the molecular ion m/z 158 (79 Br $^-$) selected in the first quadrupole and its fragment at m/z 79 (79 Br $^-$) in the second quadrupole resulting from collisional dissociation. Additional scans are collected where the first quadrupole is scanned from m/z 30–500 and the second quadrupole passes all ions to verify the isotopic patterns of Br_{2(g)}, i.e., a ratio of peak intensities of 1:2:1 at m/z 158, 160, and 162. In each experiment, API-MS samples are passed for 2–3 min through an annular denuder (URG Corp.) coated with K₂CO₃ (EM Science, \geq 99.0%) and glycerol (EM Science, 99.5%) to remove halogen gases. Any signal from the remaining aerosols accounts for background Br₂ formed in the API-MS corona discharge and is subtracted from the total Br₂ signal to yield the signal for gaseous Br₂.

While sampling with SMPS and API-MS, a small port on the chamber is opened to a collapsible Teflon chamber containing pure air at the same RH. This reservoir enables sampling without changing the overall chamber pressure. Sample flow rates into

Table 1Comparison of initial conditions used in the MAGIC simulations.

	Units	Chamber experiments					Nissenson et al. (2009) ^c	
		Case A	Case B	Case C	Case D	MBL case ^{a,b}		
[Br ⁻ (aq)]0 ^d	M	5.79	6.31	6.09	5.92	8.1×10^{-3}	5.8	
$[Na^{+}_{(aq)}]_0^d$	M	5.79	6.31	6.09	5.92	4.5	5.8	
$[O_{3(g)}]_0$	ppmv	1.55	1.65	1.66	1.95	0.020	1.5	
$[CO_{2(g)}]_0$	ppmv	1.42	3.00	2.53	1.44	394	10	
RH	%	69.1	65.0	66.7	68.0	80	69	
Aerosol: ^{e,f}								
Number concentration	10 ⁵ #/cm ³	3.32	1.74	0.80	0.71	0.92×10^{-4}	2.5	
Surface area	$10^{-3} \text{ cm}^2/\text{cm}^3$	1.03	0.42	0.30	0.15	0.13×10^{-2}	0.98	
Volume	$10^{-9} \text{ cm}^3/\text{cm}^3$	8.76	3.40	2.93	1.26	2.06×10^{-1}	10.7	
Median diameter	nm	216	186	226	170	440	234	

- ^a Initial Br⁻ concentration for the MBL case is a modeling calculation reported by Sander and Crutzen (1996) in ambient air at 76% RH.
- b Initial Na⁺ concentration for the MBL case is based on Na⁺/Br⁻ ratio in sea water and its reported conservation in fresh sea-salt aerosols (Gabriel et al., 2002).
- ^c Initial conditions from Nissenson et al. (2009) are not based on experimental observations. A log-normal particle size distribution with a median aerosol diameter of 234 nm and geometric standard deviation of 1.9 is used.
- Initial [Na⁺(aq)] and [Br⁻(aq)] in the particles for cases A–D and Nissenson et al. (2009) are based on water activity data of Cohen et al. (1987).
- e Aerosol data for cases A—D are an average of measurements taken at the beginning and end of the photolysis period. Data beyond the upper limit of the size range of the SMPS are estimated by fitting an exponential curve to the tail of the measured number concentration.
- f Aerosol size distribution for the MBL case is calculated from the equations of O'Dowd et al. (1997), which are derived by fitting a tri-modal log-normal curve to field measurements obtained in the marine boundary layer and are a function of wind speed. The global average wind speed measured at 10 m over the ocean, 6.64 m s⁻¹ (Archer and Jacobson, 2005), is used to calculate the aerosol distribution. Sea-salt aerosol size also is a function of RH, which O'Dowd et al. assume to be 80%, a typical value in the marine boundary layer (Ayers et al., 1996; Fridlind and Jacobson, 2000; Lewis and Schwartz, 2004). Aerosol pH is kept constant at 5 in the MBL case, a value consistent with sea-salt aerosol pH observed in field measurements (Fridlind and Jacobson, 2000; Pszenny et al., 2004) and used in previous modeling studies (Sander and Crutzen, 1996; Keene et al., 1998; von Glasow and Sander, 2001; von Glasow et al., 2002).

these instruments are measured to account for dilution and are used in the kinetics modeling discussed below.

2.2. MAGIC model

MAGIC is a multiphase, chemical kinetics box model used to determine the mechanisms responsible for the observed bromine production from deliquesced NaBr aerosols. A detailed description of the MAGIC model is provided elsewhere (Knipping et al., 2000; Knipping and Dabdub, 2002; Hunt et al., 2004; Thomas et al., 2006; Nissenson et al., 2008, 2009). Briefly, MAGIC considers 15 gas-phase species and 34 aqueous-phase species, 9 of which may be transferred between the two phases (see Supplementary Table 1 for a list of all species). The model contains a comprehensive treatment of gas-phase, aqueous-phase, and interfacial chemistry, including 38 gas-phase reactions, 123 aqueous-phase reactions, 9 mass accommodation coefficients, 9 Henry's law constants, 10 acid-base equilibrium constants, 2 interfacial reactions, and a kinetic salt effect parameter. Non-reactive uptake is determined using Schwartz's mass transfer model to account for limitations due to gas-phase diffusion and reactant collisions on the aerosol surface (Schwartz, 1986). Aqueous-phase diffusion and acid-base equilibrium are also considered. Activity coefficients are calculated using the ion interaction approach and the kinetic salt effect is estimated using Debye-Hückel-Brønsted equations.

Measurements of the aerosol size distribution obtained from the SMPS before and after the photolysis period are used to calculate an average aerosol size distribution for the simulations because the majority of $\mathrm{Br}_{2(g)}$ production occurs under irradiation. Aerosol data beyond the upper limit of the detectable size range of the SMPS are estimated by fitting an exponential curve to the tail of the measured aerosol size distribution. The measured particle number concentrations are summed with the fitted curve values for a total number concentration ranging from 19 nm to 5000 nm in diameter. Although in the experiment some aerosol is lost to the chamber walls and by sampling the chamber contents, the characteristics of the aerosol distribution (i.e., number concentration, total aerosol surface area, and total aerosol liquid water content) remain essentially constant during the simulations. The potential error

introduced into the model by these assumptions is discussed in Section 3.2.2.2.

There are two physical loss pathways specific to the experiment: (1) The measurements of $Br_{2(g)}$ and particle concentration require flowing some of the chamber contents through the API-MS and aerosol sampling instruments and replacing this flow from the attached collapsible Teflon chamber of humid air, which dilutes the air/particle mixture in the chamber. This dilution is modeled as a first-order loss that decreases gas-phase concentrations (Knipping and Dabdub, 2002). The rate constant for dilution is calculated from the chamber volume and the measured flow rate into each instrument and is in agreement with O₃ concentrations measured before and after sampling; (2) After the light period, the $Br_{2(g)}$ concentration declines more rapidly than predicted by known gasand aqueous-phase chemistry due to wall loss. The loss of $\text{Br}_{2(g)}$ to the walls is modeled as a first-order loss with a rate constant determined by fitting an exponential curve to the measured Br_{2(g)} data following the UV period. In the sensitivity studies, the mean wall loss rate is the average from all experiments modeled.

2.3. Uncertainty ranges for input parameters

There are 191 input parameters in MAGIC (gaseous, aqueous, and interfacial reaction rate constants, Henry's law coefficients, mass accommodation coefficients, acid—base equilibrium constants, and a kinetic salt effect parameter) that affect bromine production to varying degrees. Most of the uncertainty ranges used in this study were established by Nissenson et al. (2009), with the notable exceptions of interface reaction (1) and the photolysis rate constants (see Supplementary Table 2).

This study considers two interfacial reactions between a surface-bound bromide ion and a gas-phase species A ($A = O_3$ or OH) in reactions (1) and (2). MAGIC calculates the interface reaction rate, $R_{\rm int}$, using Schwartz's mass transfer theory (Schwartz, 1986), in which the interface reaction rate is given by,

$$R_{\rm int} = \left(\frac{r^2}{3D_{\rm g}} + \frac{4r}{3\nu\gamma}\right)^{-1} \left[A_{\rm (g)}\right],\tag{3}$$

where r is the aerosol radius, $D_{\rm g}$ the gas-phase diffusion coefficient, v the mean molecular speed of $A_{\rm (g)}$, and γ the overall surface reaction probability. In turn, γ is given by,

$$\gamma = \phi \gamma' b \Big[B r_{(aq)}^{-} \Big], \tag{4}$$

where [Br⁻(aq)] is the aqueous-phase bromide concentration, *b*[Br⁻ $_{
m (aq)}]$ is the fraction of the droplet surface covered by bromide ions, ϕ the average number of contacts between gaseous A and surfacebound Br⁻ per gas-liquid collision event, and γ' the probability that surface-bound Br and gaseous A will undergo chemical reaction upon contact. Following Thomas et al. (2006), b and ϕ are set to 0.07 M⁻¹ and 2, respectively, on the basis of molecular dynamics simulations. Therefore, only γ' in Eq. (4) is varied in MAGIC. For the reaction between O_{3(g)} and Br⁻(surf), the mean and uncertainty range of γ' are determined by adjusting this parameter (γ') in all four experiments during the initial dark period to provide the best fit to the Br_{2(g)} measurements. The present study calculates that γ' is $(0.90 \pm 0.52) \times 10^{-6}$ (all uncertainty ranges reported in this article are one standard deviation). Using 0.07 M^{-1} , 2, and 6 M for b, ϕ , and [Br $^-\text{(aq)}$], results in a value of $\gamma = (0.76 \pm 0.44) \times 10^{-6}.$ This value is within the overlapping uncertainty and hence is not significantly different from $\gamma = (1.9 \pm 0.8) \times 10^{-6}$ reported by Hunt et al. (2004).

No data are available for the value of γ' for reaction (2). However, it is expected this reaction is at least as fast as the analogous chloride reaction between gaseous OH and surface-bound Cl⁻. Laskin et al. (2006) report a lower limit for the chloride reaction rate corresponding to a γ' of 0.2 (obtained by converting γ_{net} from Laskin et al. to γ' , then dividing by two to account for the uncertainty factor of two in γ_{net}). Therefore, 0.6 \pm 0.4 is chosen for γ' in reaction (2) which covers the full range of possible values of γ' (0.2–1.0).

As discussed in the previous section, the loss of gaseous bromine to the walls of the reaction chamber is determined by a first order fit to the experimental data. The mean and uncertainty range of this rate constant are obtained by calculating the average and standard deviation of the measured wall loss rates from the four experiments.

Photolysis rate constants are established by examining the rate of ozone photolysis during experiments in which no aerosol is present in the reaction chamber. An uncertainty range of 15% is determined from these blank experiments.

2.4. Latin Hypercube sampling

The Latin Hypercube sampling technique used in this study is described in detail elsewhere (McKay et al., 1979; Derwent and Høv, 1988; Rodriguez and Dabdub, 2003; Nissenson et al., 2008, 2009). Briefly, all input parameters are treated as random variables with a log-normal probability distribution, except for the kinetic salt effect parameter which has a uniform probability distribution as in Nissenson et al. (2008). Each probability distribution is divided into n independent intervals of equal probability, and a single value of the input parameter is selected randomly from each interval. Then, for every input parameter, each of the n values is assigned randomly to one of the n input parameter samples, each of which is used for a simulation in MAGIC. The number of simulations is sufficiently large (n=5000) to ensure reliable analysis; a pilot investigation found no significant differences in the results from a doubling of n.

2.5. Sensitivity and uncertainty analyses

The relationship between the input parameters and bromine production is determined by analyzing the raw output from MAGIC

using multiple linear regression. Each input parameter's regression coefficient (β_i) represents the change in $\mathrm{Br}_{2(g)}$ output per unit increase in that input parameter, with all other input parameters held constant, at a chosen analysis time. The magnitude of an input parameter's regression coefficient is a measure of the sensitivity of $[\mathrm{Br}_{2(g)}]$ to changes in that parameter, relative to all other parameters. The value of β is calculated at different times to examine how the sensitivity of $\mathrm{Br}_{2(g)}$ output to different chemical and physical mechanisms evolves during the simulations.

Multiple linear regression assumes that the input parameters are independent of each other and that the gaseous bromine concentration is linearly dependent upon the input parameters over their range of uncertainties. The regression coefficients are assumed independent of the input parameter's uncertainty ranges only in the asymptotic (infinite-sample) limit, which is accounted for here by a large sample of simulations.

The contribution that input parameter i makes to the variance of the peak bromine concentration is given by u_i in the error propagation formula,

$$u_{i} = \frac{\left(\sigma_{i}\beta_{i}/x_{i}^{*}\right)^{2}}{\sum_{k=1}^{n}\left(\sigma_{k}\beta_{k}/x_{k}^{*}\right)^{2}} \times 100\%, \tag{5}$$

where x_i^* and σ_i are the mean and standard deviation of input parameter i, respectively.

The reader is referred to Nissenson et al. (2008) and Nissenson et al. (2009) for a detailed explanation of how the regression coefficients are calculated and for additional details regarding the error propagation.

3. Results

3.1. Chamber experiments

In the chamber experiments, deliquesced NaBr aerosols are exposed to ozone and UV light. Aerosol properties, such as total aerosol surface area and total aerosol volume, are varied to study how changes in the availability of bromide in the system affect $Br_{2(g)}$ production. Other initial conditions such as relative humidity, concentrations of $O_{3(g)}$ and $CO_{2(g)}$, and the concentration of NaBr in the aerosols are similar among experiments (see Table 1, cases A–D)

The concentrations of $Br_{2(g)}$, $BrO_{(g)}$, and $O_{3(g)}$ measured during the experiments are presented in Fig. 1 for cases B and D (concentrations measured in cases A and C are shown in Supplementary Fig. 1). In all cases A—D during the 40—60 min initial dark period, $Br_{2(g)}$ is produced slowly, $BrO_{(g)}$ levels are negligible, and the concentration of $O_{3(g)}$ decreases slowly due to reaction with bromide, wall loss, and the dilution of the chamber contents from sampling.

When the UV lamps are turned on, the concentration of $Br_{2(g)}$ rises quickly, increasing by an order of magnitude in a few minutes. During this time period, the rate of $Br_{2(g)}$ production is much faster than the rate $Br_{2(g)}$ is lost to the walls (lifetime with respect to wall loss $\sim 56\,$ min). Gaseous BrO levels reach their peak faster than $Br_{2(g)}$ and then decline before the end of the irradiation period. The concentration of ozone decreases rapidly due to photolysis and through reaction with atomic bromine.

Following approximately 10 min of UV irradiation, the photolysis lamps are turned off and the system starts a second dark period. The bromine explosion mechanism shuts down due to a lack of UV light and the slope of the $[Br_{2(g)}]$ curve shifts from positive (or near zero) to negative. The concentration of $BrO_{(g)}$ rapidly falls to negligible levels due to its high reactivity.

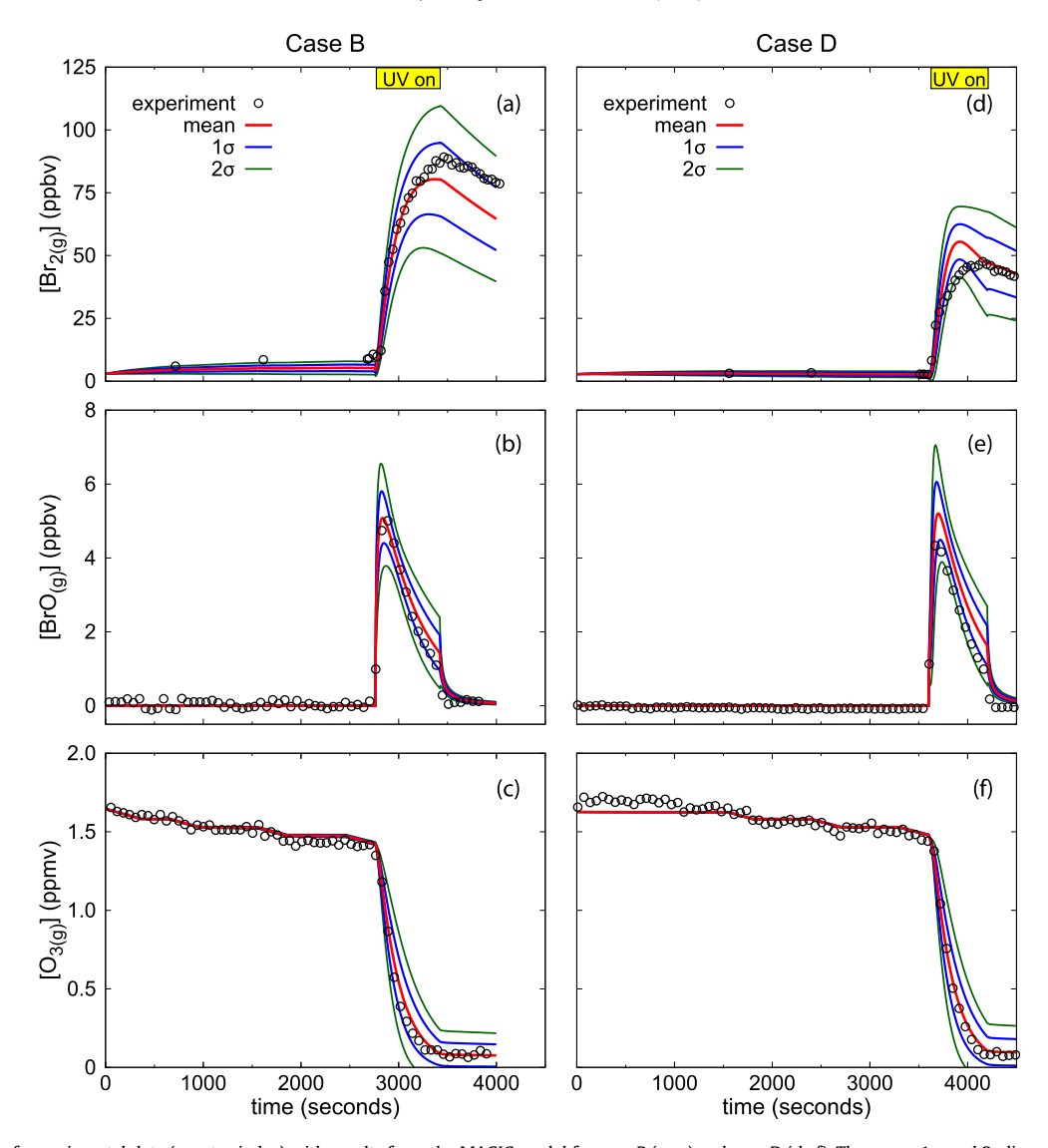


Fig. 1. A comparison of experimental data (empty circles) with results from the MAGIC model for case B (a–c) and case D (d–f). The mean, 1σ , and 2σ lines are based on the 5000 simulations from the sensitivity analysis performed on MAGIC for each case. The UV lamps are turned on for 660 s in case B and 600 s in case D.

3.2. Computer modeling

Four sets of simulations are conducted with MAGIC using the conditions measured during the four experiments (cases A, B, C, and D). An additional scenario is examined using conditions that are more representative of the remote marine boundary layer (MBL case, discussed in Section 3.2.3). The sensitivity analysis of the MAGIC model investigates how varying the input parameters may affect the release of $\text{Br}_{2(g)}$ from NaBr aerosols.

The observed concentrations of $Br_{2(g)}$, $BrO_{(g)}$, and $O_{3(g)}$ measured during the four experiments are compared with model predictions from the sensitivity analyses in order to test MAGIC. Fig. 1 compares the experimental measurements to the model predictions of the mean, 1σ , and 2σ values of $Br_{2(g)}$, $BrO_{(g)}$, and $O_{3(g)}$ for all 5000 simulations for cases B and D (similar plots for cases A and C are shown in Supplementary Fig. 1). Most of the measured values of $Br_{2(g)}$, $BrO_{(g)}$ and $O_{3(g)}$ fall well within 2σ lines predicted by MAGIC and all model predictions show the same qualitative behavior, demonstrating that the important mechanisms in the bromine explosion pathway are included in MAGIC.

Previous studies under dark conditions showed that the reaction of O_3 with $Br^-_{(aq)}$ at the particle interface dominates $Br_{2(g)}$

production (Hunt et al., 2004; Nissenson et al., 2009). This study finds that interface reaction (1) dominates $Br_{2(g)}$ production during the initial dark period, consistent with Hunt et al. (2004) and Nissenson et al. (2009). When this reaction is excluded from MAGIC, gaseous bromine levels in the dark drop by a factor of 3–5. However, $Br_{2(g)}$ is produced rapidly when the UV lamps are turned on, indicating that a different mechanism is responsible for most of the bromine production during the UV period. Sensitivity analyses conducted on the MAGIC model identify the rate-limiting steps in the bromine explosion pathway while the uncertainty analyses identify the input parameters that produce the most uncertainty in model predictions of $Br_{2(g)}$.

3.2.1. Comparison to Nissenson et al. (2009)

Nissenson et al. (2009) conducted a limited sensitivity study on MAGIC using initial conditions similar to case A (Table 1). That study primarily focused on the sensitivity of bromine output at peak $[Br_{2(g)}]$ to input parameters in order to examine how these parameters affect the maximum output of bromine. It was found that the rate-limiting steps in bromine production did not change once peak $[Br_{2(g)}]$ occurred, but the rate-limiting steps at times prior to peak $[Br_{2(g)}]$ were not examined. The present study

expands upon the work of Nissenson et al. (2009) by examining the sensitivity of bromine production at peak [Br_{2(g)}] and at times prior to the peak (e.g., 60 s after the UV lamps are turned on). Chamber conditions in the current study are based on experimental observations (cases A–D), while Nissenson et al. (2009) used representative conditions not backed by measurements in their simulations. Additionally, measurements of Br_{2(g)}, BrO_(g), and O_{3(g)} taken from the chamber experiments are used to constrain and test the model in this study, while Nissenson et al. (2009) only attempted to achieve qualitative agreement between simulations and unpublished data from chamber experiments.

Table 2 compares the regression coefficients calculated for Nissenson et al. (2009) to this study at peak $[Br_{2(g)}]$. Input parameters are selected based on their relatively high value or their importance in Nissenson et al. (2009). As described in Section 2.5, the magnitude of a regression coefficient (β) is a measure of the sensitivity of the predicted Br_{2(g)} concentration to an input parameter and is used to identify the rate-limiting steps in bromine production. A positive regression coefficient means bromine levels would be enhanced if the input parameter were increased, while a negative regression coefficient means bromine levels would decline if the input parameter were increased. Peak $[Br_{2(\sigma)}]$ is most sensitive to many of the same chemical and physical processes in both Nissenson et al. (2009) and cases A-C, despite having significantly different initial conditions. This indicates the rate-limiting steps in maximum bromine production for these four scenarios are similar.

The bromine explosion is initiated when the UV lamps are turned on (Hausmann and Platt, 1994). Gaseous ozone photolyzes readily at 254 nm, producing O_X and HO_X radicals,

$$O_{3(g)} + h\nu \rightarrow O(^{1}D)_{(g)} + O_{2(g)},$$
 (6)

$$O(^{1}D)_{(g)} + H_{2}O_{(g)} \rightarrow 2 OH_{(g)},$$
 (7)

$$O(^1D)_{(g)} + N_{2(g)} \rightarrow O(^3P)_{(g)} + N_{2(g)}, \tag{8} \label{eq:8}$$

$$O(^{1}D)_{(g)} + O_{2(g)} \rightarrow O(^{3}P)_{(g)} + O_{2(g)},$$
 (9)

$$O_{3(g)} + OH_{(g)} \rightarrow HO_{2(g)} + O_{2(g)}.$$
 (10)

These radicals are involved in some of the key gas-phase reactions involving brominated species,

$$OH_{(g)} + Br_{2(g)} \rightarrow HOBr_{(g)} + Br_{(g)}, \tag{11}$$

$$HO_{2(g)} + BrO_{(g)} \rightarrow HOBr_{(g)} + O_{2(g)},$$
 (12)

$$Br_{(g)} + O_{3(g)} \rightarrow BrO_{(g)} + O_{2(g)},$$
 (13)

$$BrO_{(g)} + BrO_{(g)} \rightarrow 2 Br_{(g)} + O_{2(g)},$$
 (14)

$$BrO_{(g)} + BrO_{(g)} \rightarrow Br_{2(g)} + O_{2(g)}.$$
 (15)

The uptake of HOBr into the aqueous phase leads to the production of $Br_{2(aq)}$ through the reactions,

$$HOBr_{(aq)} + Br_{(aq)}^{-} + H_2O_{(aq)} \rightarrow Br_{2(aq)} + OH_{(aq)}^{-} + H_2O_{(aq)},$$
 (16)

$$HOBr_{(aq)} + Br_{(aq)}^{-} + HCO_{3(aq)}^{-} \rightarrow Br_{2(aq)} + CO_{3(aq)}^{2-} + H_2O_{(aq)}$$
 (17)

while the reverse reactions of (16) and (17) destroy aqueous bromine

$$Br_{2(aq)} + OH_{(aq)}^{-} + H_2O_{(aq)} \rightarrow HOBr_{(aq)} + Br_{(aq)}^{-} + H_2O_{(aq)},$$
 (18)

$$Br_{2(aq)} + CO_{3(aq)}^{2-} + H_2O_{(aq)} \rightarrow HOBr_{(aq)} + Br_{(aq)}^- + HCO_{3(aq)}^-.$$
 (19)

As bromine levels increase in the aqueous-phase, the deviation from Henry's law equilibrium drives Br₂ into the gas-phase.

Table 2 shows that in both Nissenson et al. (2009) and cases A–C, peak $[Br_{2(g)}]$ is most sensitive to gas-phase reactions, such as the BrO self-reactions (14 and 15) and ozone photolysis. In addition, $[Br_{2(g)}]$ is relatively insensitive to interfacial reactions, aqueous

Table 2 Selected regression coefficients (β) calculated at peak [Br_{2(g)}] from Nissenson et al. (2009) and this study (cases A–D).

Input parameter ^a	Nissenson et al. (2009) ^b	Case A	Case B	Case C	Case D
Interface reaction probability (γ')					
$O_{3(g)} + Br_{(surf)}^{-} \rightarrow 0.5 Br_{2(g)} + O_{3(aq)}^{-}(R1)$	0.05	0.05	0.02	0.01	NC ^c
$OH_{(g)} + Br_{(surf)}^{-} \rightarrow 0.5 Br_{2(g)} + OH_{(aq)}^{-} (R2)$	0.03	0.05	0.02	0.01	0.04
Reaction rate constants					
$O_{3(g)} + h\nu \rightarrow O(^{1}D)_{(g)} + O_{2(g)}(R6)$	0.06	0.23	0.22	0.21	NC
$O(^{1}D)_{(g)} + H_2O_{(g)} \rightarrow 2OH_{(g)}(R7)^d$	0.03	0.21	0.19	0.18	NC
$O(^{1}D)_{(g)} + N_{2(g)} \rightarrow O(^{3}P)_{(g)} + N_{2(g)} (R8)^{d}$	-0.03	-0.15	-0.14	-0.14	NC
$OH_{(g)} + Br_{2(g)} \rightarrow HOBr_{(g)} + Br_{(g)} (R11)^e$	-0.02	0.04	NC	NC	0.07
$HO_{2(g)} + BrO_{(g)} \rightarrow HOBr_{(g)} + O_{2(g)}(R12)$	0.05	0.04	NC	0.05	0.04
$2BrO_{(g)} \rightarrow 2Br_{(g)} + O_{2(g)}(R14)$	-0.57	-0.49	-0.49	-0.44	-0.04
$2BrO_{(g)} \rightarrow Br_{2(g)} + O_{2(g)}(R15)$	0.56	0.47	0.46	0.41	0.04
$HOBr_{(aq)} + Br_{(aq)}^{-} + H_2O_{(aq)} \rightarrow Br_{2(aq)} + OH_{(aq)}^{-} + H_2O_{(aq)}$ (R16)	0.03	0.05	0.04	0.06	0.14
$Br_{2(aq)} + OH^{-}_{(aq)} + H_2O_{(aq)} \rightarrow HOBr_{(aq)} + Br^{-}_{(aq)} + H_2O_{(aq)} (R18)^d$	-0.02	-0.04	-0.03	-0.04	-0.07
Mass accommodation coefficients					
$\alpha(HO_2)$	-0.03	-0.03	-0.03	-0.03	-0.06
Henry's law constants					
$H(Br_2)$	-0.04	-0.06	-0.06	-0.07	-0.15
H(HOBr) ^d	0.01	0.02	0.03	0.05	0.11
H(CO ₂)	0.03	0.04	0.03	0.03	0.09

^a Reactions that are numbered in the main text of this study are listed with their reaction numbers in parentheses.

Results from Nissenson et al. (2009) are from the "LightT600" scenario.

 $^{^{}c}$ NC = not significantly correlated with peak [Br_{2(g)}], p-value > 0.05.

d This input parameter was calculated but not reported in Nissenson et al. (2009).

e The negative regression coefficient for R11 in Nissenson et al. (2009) is a result of a lower O_3 concentration at the time of the peak $[Br_{2(g)}]$ in that study, such that the recycling of bromine-containing species into Br_2 , which is initiated by reaction of O_3 , is overwhelmed by the destruction of Br_2 by R11.

reactions, and input parameters associated with mass transfer, such as Henry's law coefficients and mass accommodation coefficients. Thus, maximum bromine production in these systems is limited by gas-phase chemistry.

One notable difference between cases A–C and Nissenson et al. (2009) is that in cases A–C peak $[Br_{2(g)}]$ is much more sensitive to reactions (6–8), which involve the photolysis of ozone and the production of HO_x radicals. This difference in regression coefficients likely is due to the use of a different photolysis rate constant for ozone in cases A–D compared to Nissenson et al. (2009); in the present study, the photolysis rate constant for ozone is obtained from experimental data and is 55% lower than the photolysis rate constant used in Nissenson et al. (2009). Despite this difference, peak $[Br_{2(g)}]$ in cases A–C and in Nissenson et al. (2009) is most sensitive to the BrO self-reactions (14 and 15), indicating that gasphase chemistry is rate limiting under these conditions.

By contrast, in case D peak $[Br_{2(g)}]$ is much more sensitive to aqueous reactions that produce (reaction 16) and destroy (reaction 18) $Br_{2(aq)}$, the mass accommodation coefficient of HO₂, and the Henry's law coefficients for Br_2 , HOBr and CO_2 . Maximum bromine production in case D is therefore limited by aqueous bromine production and mass transfer. Section 3.2.2 explores the differences between cases A–C and case D in greater detail.

3.2.2. Ozone-limited regime (cases A—C) vs bromide-limited regime (case D)

Table 2 shows that the rate-limiting steps in peak [Br_{2(g)}] formation for cases A—C are significantly different than for case D. It will be shown that this difference is due primarily to the amount of ozone and bromide initially in the system when the UV lamps are turned on. Gaseous ozone and bromide are key reactants in the bromine explosion mechanism discussed in the previous section and both species are necessary for bromine production. In all four cases, ozone is depleted during the UV period primarily through photolysis and reaction (13) with atomic bromine (Fig. 1 and Supplementary Fig. 1). However, Fig. 2 shows that most of the bromide still resides in the aerosols at the end of the UV period in cases A—C, while bromide is depleted well before the end of the UV period in case D.

Two additional simulations are conducted for cases B and D using the nominal (mean) values of the input parameters in which $[O_{3(g)}]_0$ and $[NaBr_{(aq)}]_0$ are enhanced by 20%. Fig. 3a shows that the peak concentration of $Br_{2(g)}$ in case B increases much more with the addition of $O_{3(g)}$ (\sim 19% increase in $[Br_{2(g)}]_{peak}$) than with the addition of NaBr_{(aq)} (\sim 1% increase in $[Br_{2(g)}]_{peak}$). Similar results are observed for cases A and C, indicating cases A—C are in an ozone-limited regime. In contrast, Fig. 3b shows that the peak concentration of $Br_{2(g)}$ in case D increases much less with the addition of $O_{3(g)}$ (<1% increase in $[Br_{2(g)}]_{peak}$) than with the addition of NaBr_{(aq)} (\sim 19% increase in $[Br_{2(g)}]_{peak}$), further supporting that case D is in a bromide-limited regime.

Table 1 shows that cases A–D initially have similar concentrations of ozone and bromide, but case D contains the least amount of total bromide because it has the lowest total aerosol volume. Additional simulations described in Supplementary Material are conducted to assess the sensitivity of peak $[Br_{2(g)}]$ to variations in aerosol number concentration, total surface area, and total aerosol volume. As expected, raising the aerosol number concentration (without adjusting the shape of the aerosol size distribution) increases the total bromide in the system and enhances peak $Br_{2(g)}$ significantly in the Br^- -limited system (case D) but negligibly in an O_3 -limited system (case B). Interestingly, varying total aerosol surface area while leaving total aerosol volume constant does not impact peak $[Br_{2(g)}]$ levels, meaning it is the reduction in aerosol

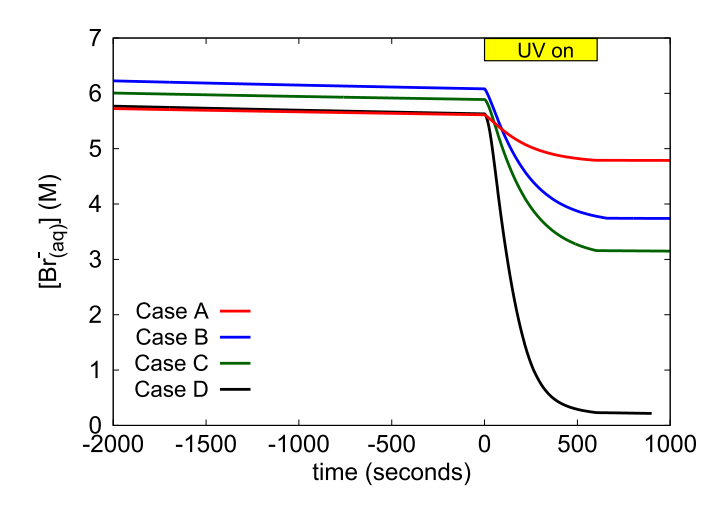


Fig. 2. Concentration of aqueous bromide for cases A, B, C, and D predicted by the MAGIC model using the nominal (mean) values for the input parameters. The data lines are shifted in time so that t=0 s corresponds to the moment when the UV lamps turn on for easier comparison. The UV lamps are turned on for 600 s in cases A, C, and D. and 660 s in case B.

volume (the total bromide in the system), not surface area, that causes case D to differ from cases A—C.

3.2.2.1. Time dependence of regression coefficients. The regression coefficients calculated at peak $[Br_{2(g)}]$ in Table 2 determine the sensitivity of maximum bromine production to the various chemical and physical mechanisms in the system, and identify the ratelimiting steps in maximum bromine production. However, the concentration of many species change rapidly during the UV period and the rate-limiting steps in bromine production change during this time as well. Fig. 4 demonstrates the time evolution of the regression coefficients for an ozone-limited system (represented by case B because of its intermediate aerosol parameters) and a bromide-limited system (case D). Results for cases A and C, both ozone-limited, are similar to case B and are shown in Supplementary Fig. 2.

At the beginning of the UV period, when ample ozone and bromide are present, predicted $[Br_{2(g)}]$ in both cases B and D is quite sensitive to gas-phase reactions that determine $OH_{(g)}$ levels. Gaseous bromine levels are positively correlated with reactions that lead to $OH_{(g)}$ formation, such as ozone photolysis (reaction 6) and reaction of $O(^1D)_{(g)}$ with $H_2O_{(g)}$ (reaction 7), and negatively correlated with reactions that prevent $OH_{(g)}$ formation, such as the $O(^1D)_{(g)}$ quenching reactions (8) and (9). Reaction (10) also is negatively correlated with gaseous bromine levels since this reaction destroys both gaseous ozone and OH.

MAGIC predicts that at the onset of photolysis, $Br_{2(g)}$ levels drop for ~ 5 s due to reaction (11) with $OH_{(g)}$ before making a rapid recovery. This decrease is not observed experimentally due to its short duration. Although reaction (11) momentarily destroys $Br_{2(g)}$, it initially has a strong positive correlation with $[Br_{2(g)}]$ because it produces $HOBr_{(g)}$, a key species in liberating bromide from NaBr aerosols; reaction (11) is the main source of $HOBr_{(g)}$ during the UV period. The reaction of $HO_{2(g)}$ with $BrO_{(g)}$ (reaction 12) is an important secondary source of $HOBr_{(g)}$ and also has a strong positive correlation with $[Br_{2(g)}]$ initially.

During the first several hundred seconds after the UV lamps are turned on, there is sufficient ozone and bromide to fuel the rapid production of $Br_{2(g)}$ through the bromine explosion mechanism. However, increasing $Br_{2(g)}$ levels leads to enhanced catalytic destruction of ozone via reactions (13) and (14); in all four cases,

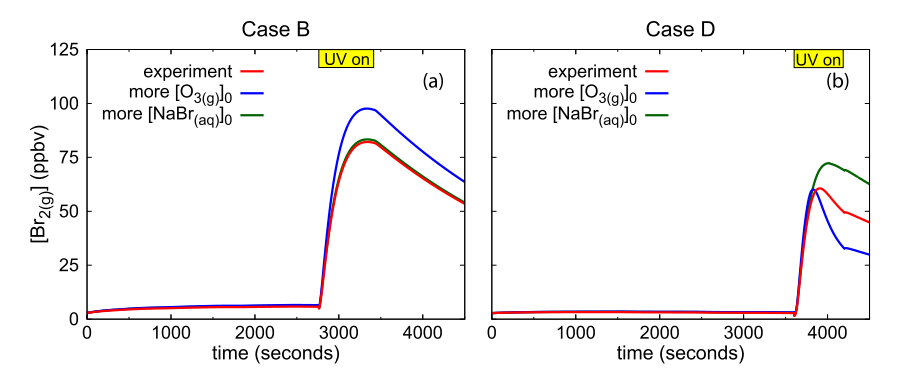


Fig. 3. Concentration of $Br_{2(g)}$ predicted by the MAGIC model (with nominal values for the input parameters) using different initial conditions for (a) case B and (b) case D. The "experiment" simulations use the values of $[O_{3(g)}]_0$ and $[NaBr_{(aq)}]_0$ measured during experiments B and D. In the "more $[O_{3(g)}]_0$ " simulations, $[O_{3(g)}]_0$ is increased by 20% while $[NaBr_{(aq)}]_0$ " is unchanged. In the "more $[NaBr_{(aq)}]_0$ " simulations, $[NaBr_{(aq)}]_0$ is increased by 20% and $[O_{3(g)}]_0$ is unchanged. The UV lamps are turned on for 660 s in case B and 600 s in case D.

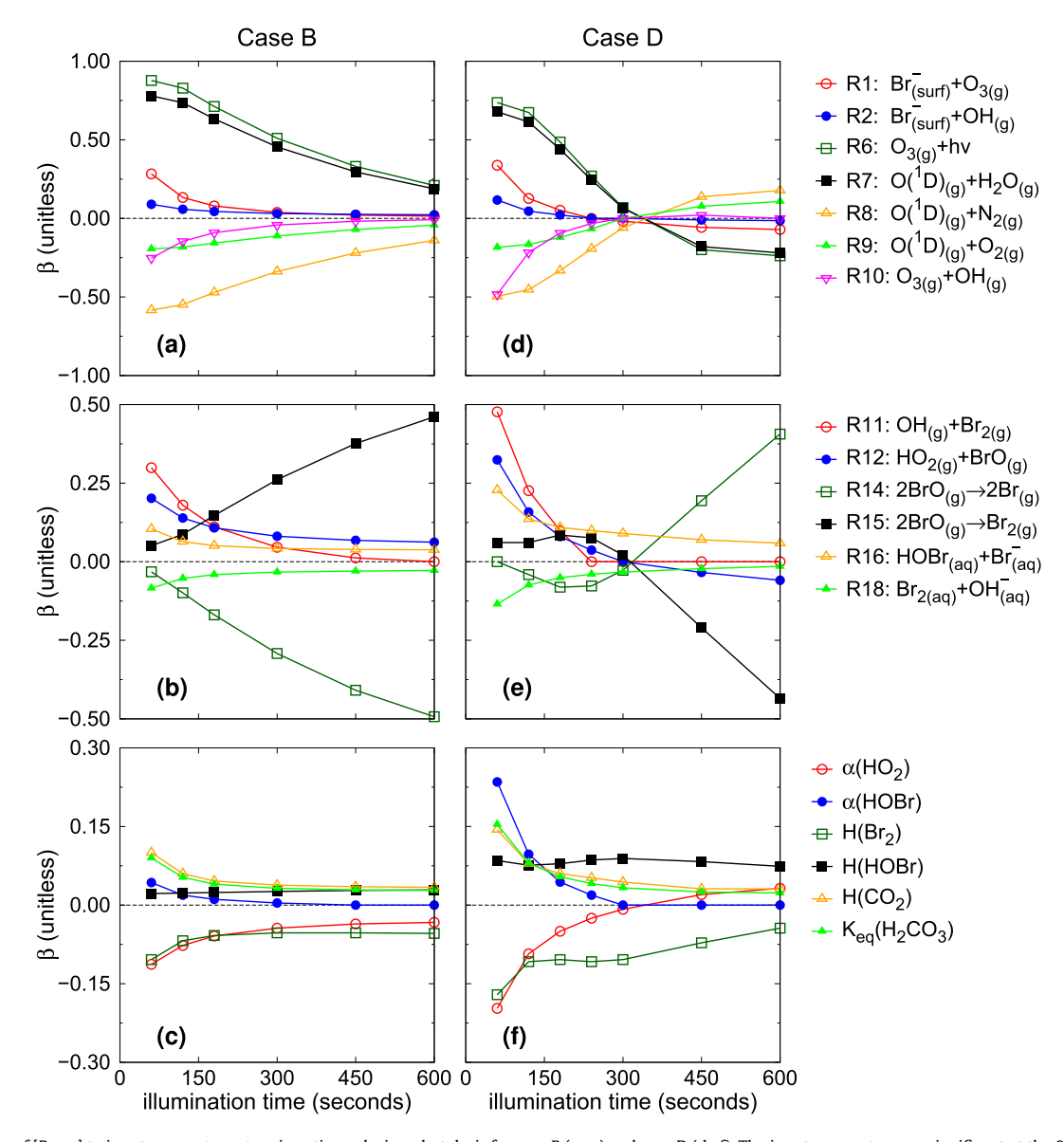


Fig. 4. Sensitivity of $[Br_{2(g)}]$ to input parameters at various times during photolysis for case B (a-c) and case D (d-f). The input parameters are significant at the 0.05 level and have either a regression coefficient greater than 0.2 for at least one analysis time or are deemed interesting by the authors. Zero seconds corresponds to when the UV lamps are turned on. Reaction rate constants are represented by R followed by the chemical reaction number from the text. $R_{eq}(X)$, $R_{eq}(X)$, $R_{eq}(X)$, represent the acid—base equilibrium constant, Henry's law constant, and mass accommodation coefficient of species $R_{eq}(X)$, respectively.

the total amount of ozone destroyed via reaction (13) with $Br_{(g)}$ is 3–8% greater than through photolysis and reaction with HO_x radicals combined. In the ozone-limited systems (cases A–C), gaseous ozone is depleted before bromide levels decline greatly. Since the $BrO_{(g)}$ self-reaction (14) enhances $Br_{(g)}$ production and reaction (15) inhibits $Br_{(g)}$ production, predicted $[Br_{2(g)}]$ in cases A–C becomes increasingly sensitive to these two reactions throughout the UV period, eventually growing to be the most important rate-limiting steps in bromine production.

In the bromide-limited system (case D), Br⁻_(aq) is the limiting reagent in the bromine explosion mechanism and processes that significantly impact $[\mathrm{Br}^-{}_{(\mathrm{aq})}]$ become the rate-limiting steps. During the first half of the UV period, Br_{2(g)} levels in case D compared to case B are $\sim 50-200\%$ more sensitive to aqueous reactions (16–18), ~200–300% more sensitive to the Henry's law constant of HOBr, $\sim 50-100\%$ more sensitive to the Henry's law constant of Br₂, ~400-600% more sensitive to the mass accommodation coefficient of HOBr, and are generally less sensitive to gas-phase reactions that produce HO_x and to the $BrO_{(g)}$ self-reactions (14) and (15). Once bromide is depleted in the aerosols in case D (by 300 s, $[Br^{-}_{(aq)}]$ has declined to ~ 10% of its original value), the pathways of Br₂ formation from reactions (16) and (17) of $HOBr_{(aq)}$ with $Br_{(aq)}^{-}$ are shut down, resulting in accumulation of bromine atoms in HOBr; HOBr_(g) levels are over an order of magnitude greater in case D than in cases A-C, despite significantly lower total bromide in case D (Table 1).

The onset of bromide depletion in the aerosols produces dramatic changes to the regression coefficients of input parameters that indirectly affect $HOBr_{(g)}$ production. Gaseous HOBr is a sink for bromine atoms and is formed primarily through reactions (11) and (12), which involve HO_X reactants. Ozone photolysis (reaction 6) and reaction (7) of $O(^{1}D)_{(g)}$ and $H_{2}O_{(g)}$, both important in HO_{x} production, become negatively correlated with Br_{2(g)} levels while the $O(^{1}D)_{(g)}$ quenching reactions (8) and (9), which reduce HO_{x} production, become positively correlated with Br_{2(g)} levels. The regression coefficients of the $BrO_{(g)}$ self-reactions (14) and (15) also change sign. Although reaction (14) plays a large role in the catalytic destruction of ozone and is negatively correlated with $Br_{2(g)}$ levels prior to bromide depletion, this reaction becomes positively correlated with Br_{2(g)} levels after bromide depletion since lower ozone levels result in reduced HO_x production and a slower rate of HOBr formation via reactions (11) and (12). Lower HOBr levels means more bromine atoms are available to form $Br_{2(g)}$ at later illumination times. Reaction (15) enhances HO_x production by converting BrO_(g) into Br_{2(g)} instead of bromine atoms, which destroy ozone via reaction (13). Greater HO_x levels result in enhanced HOBr production via reactions (11) and (12), causing reaction (15) to have a negative regression coefficient after bromide depletion. This dramatic change in several of the regression coefficients upon bromide depletion at \sim 300 s is one of the defining characteristics for case D.

Hydroxyl radicals can produce $Br_{2(g)}$ directly by reacting with bromide at the aerosol surface via reaction (2). However, this reaction is weakly correlated with $Br_{2(g)}$ levels, especially at longer times, and removal of this reaction lowers $Br_{2(g)}$ production by only a few percent. This result is in agreement with previous modeling studies by Thomas et al. (2006) and Nissenson et al. (2009) that concluded the reaction of $OH_{(g)}$ with $Br_{(surf)}$ is a minor source of $Br_{2(g)}$ production under irradiation. The interfacial reaction (1) with $O_{3(g)}$ is strongly correlated with bromine levels immediately after the lamps are turned on, but this is due to reaction (1) dominating $Br_{2(g)}$ production during the preceding dark period; insufficient time has passed for the bromine explosion to produce a significant amount of $Br_{2(g)}$. Relatively little $Br_{2(g)}$ is produced during the UV period by reaction (1), resulting

in a rapidly declining regression coefficient for this input parameter.

In summary, although the sensitivity studies show that the bromine explosion mechanism is the same for all four cases - (1) Production of HOBr in the gas-phase, (2) Uptake of HOBr into the aqueous-phase, (3) Reaction of HOBr $_{(aq)}$ with $Br^-_{(aq)}$ to produce $Br_{2(aq)}$, (4) Degassing of Br_2 from the aerosols - the rate-limiting steps differ greatly between the ozone-limited (cases A-C) and bromide-limited (case D) cases, and also change as a function of reaction time. Fig. 5a is a schematic summarizing the processes in cases A-D with the highest regression coefficients during the UV period. Additionally, the minor influence of the $OH_{(g)}-Br^-_{(surf)}$ interface reaction on Br_2 production, as predicted by Nissenson et al. (2009), is supported by experimental data under different aerosol bromide and O_3 availabilities.

3.2.2.2. Uncertainty analysis. The uncertainty analysis elucidates the input parameters that most significantly affect MAGIC's ability to predict [Br_{2(g)}] at different simulation times. Fig. 6 shows the results of the uncertainty analysis for case B (ozone-limited) and case D (bromide-limited). Results for cases A and C are similar to case B and are presented in Supplementary Fig. 3. In all four cases, interfacial reaction (1) with $O_{3(g)}$ produces the most uncertainty in bromine levels immediately after the lamps are turned on. As in the sensitivity analysis, this result is due to reaction (1) dominating Br_{2(g)} production during the preceding dark period. Note that this value is quite uncertain and further experiments to reduce the uncertainty associated with this dark interface reaction would be useful. During the early part of the UV period, the regression coefficient of interfacial reaction (1) decreases rapidly while the regression coefficient for ozone photolysis (reaction 6) and OH production via reaction (7) remain relatively high (Fig. 2). As a result, reactions (6) and (7) quickly become the greatest contributors to the model uncertainty.

As ozone is destroyed in the ozone-limited systems (cases A–C), bromine production becomes increasingly sensitive to the $BrO_{(g)}$ self-reactions (14) and (15) (Fig. 4 and Supplementary Fig. 2). The large regression coefficients on these two reactions result in their generating over 75% of the uncertainty in predicted $Br_{2(g)}$ levels by the time ozone is depleted. In bromide-limited systems (case D), gaseous bromine levels are more sensitive to aqueous bromine production via reaction (16) and the Henry's law constant of HOBr by the time bromide is depleted (\sim 300 s). At that time, the relatively large regression coefficients and uncertainty ranges of reaction (16) and H(HOBr) result in the two input parameters generating over 50% of the uncertainty in predicted $Br_{2(g)}$ levels. Following the shut down of $Br_{2(g)}$ production, the $BrO_{(g)}$ self-reactions (14) and (15) begin to dominate the uncertainty in case D due to their increasing regression coefficients.

The uncertainty analysis focuses on how uncertainties in chemical and physical processes affect MAGIC's ability to predict gaseous bromine levels. Uncertainties in the aerosol size distribution used in MAGIC also affect the total amount of bromide in the system. The sources of these errors are the uncertainty in the measurement of the aerosol size (± 5 nm) and number concentration ($\pm 20\%$) (Hunt et al., 2004), as well as the assumption that the aerosol properties do not change during the simulations. However, even with the uncertainties in the aerosol size distribution, the model successfully predicts the occurrence of a Br_{2(g)} explosion, calculates a peak Br_{2(g)} concentration that is close to the experimental value, and produces O_{3(g)} and BrO_(g) curves that are similar to measurements (see Supplementary Material for a discussion regarding how aerosol concentration, total aerosol surface, and total aerosol volume affect predicted bromine levels).

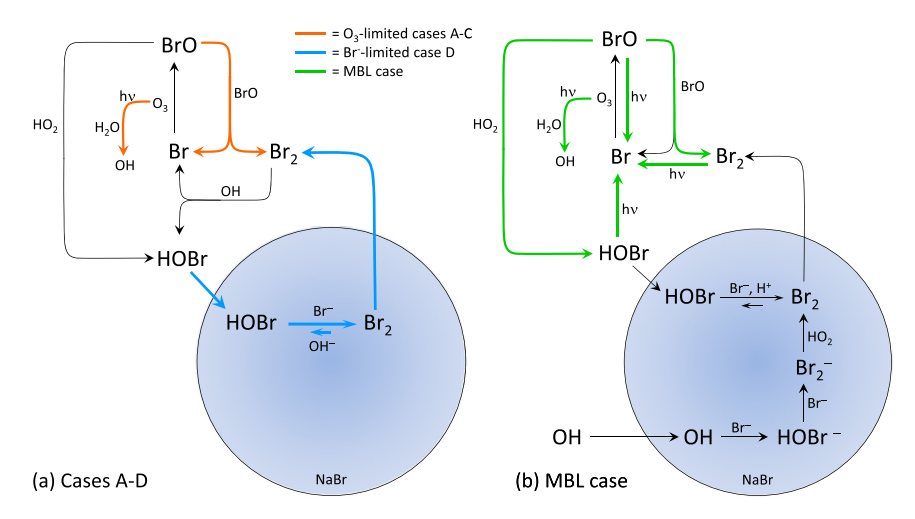


Fig. 5. A simplified schematic diagram of the key chemical and physical processes governing Br_{2(g)} levels during the UV period for (a) cases A–D and (b) the MBL case. The circular area represents the condensed phase (liquid aerosol). The processes with the largest regression coefficients at peak Br_{2(g)} are indicated for ozone-limited cases A–C, bromide-limited case D and the MBL case

3.2.3. Bromide-limited regime (case D) vs. MBL case

The conditions of the marine boundary layer are quite different than in the chamber experiments. In the remote marine boundary layer, interhalogen reactions and oxides of nitrogen also play a role in the generating gas-phase bromine from sea-salt aerosols (Vogt et al., 1996, 1999; Foster et al., 2001; Sander et al., 2003; Simpson et al., 2007; Richards and Finlayson-Pitts, 2012; Sommariva and von Glasow, 2012). Additionally, ambient sea-salt aerosols in the remote marine boundary layer are composed of a mixture of individual aerosols with different characteristics (Keene et al., 1998; Sander et al., 2003), and often have organic coatings which can enhance the rate of bromide oxidation from NaBr solutions (Clifford and Donaldson, 2007). While examining the impact of other halogens and oxides of nitrogen on brominated compounds is beyond the scope of the present work, the authors acknowledge that these exclusions from the current study limit direct extrapolation of the results to the atmosphere. For example, some reactive species that are not accounted for can affect the concentrations and time dependence of key atmospheric species such as $Br_{2(g)}$. However, in mixtures of Cl⁻ and Br⁻ characteristic of sea salt, the interhalogen chemistry drives the production of gas-phase bromine until the aqueous phase is largely depleted of Br-, at which time gas-phase chlorine compounds are formed (Abbatt, 1994; Allanic et al., 1997; Kirchner et al., 1997; Abbatt and Waschewsky, 1998; Mochida et al., 1998; Oum et al., 1998a,b; Chu and Chu, 1999; Fickert et al., 1999; Liu et al., 2001; Frinak and Abbatt, 2006; George and Anastasio, 2007; Sjostedt and Abbatt, 2008; Abbatt et al., 2010; Richards-Henderson et al., 2013). Simulations of the remote marine boundary layer using a bromide-only computer model can help identify the rate-limiting steps in the production of gaseous brominated compounds among non-interhalogen reactions. Such simulations may be used to help assess which of the four cases (A–D) examined above is most similar to the conditions and chemistry in the remote marine boundary layer, and hence which reactions discussed in this paper are more likely to be important in the atmosphere. An additional set of simulations (MBL case) is conducted for this purpose. The MBL case below simulates a parcel of air containing pure NaBr aerosols in the remote marine boundary layer during sunrise at mid-latitude.

The initial conditions of the MBL case are listed in Table 1. Initial $[O_{3(g)}]$ and $[CO_{2(g)}]$ are set to 20 ppbv (Dickerson et al., 1999; Pszenny et al., 2004; von Glasow and Crutzen, 2004; von Glasow, 2006) and 394 ppmv (Tans and Keeling, 2011), respectively. An initial bromide concentration of 8.1×10^{-3} M is used based on the calculations of Sander and Crutzen (1996) for freshly generated seasalt aerosols equilibrated with ambient air at 76% RH, with the same

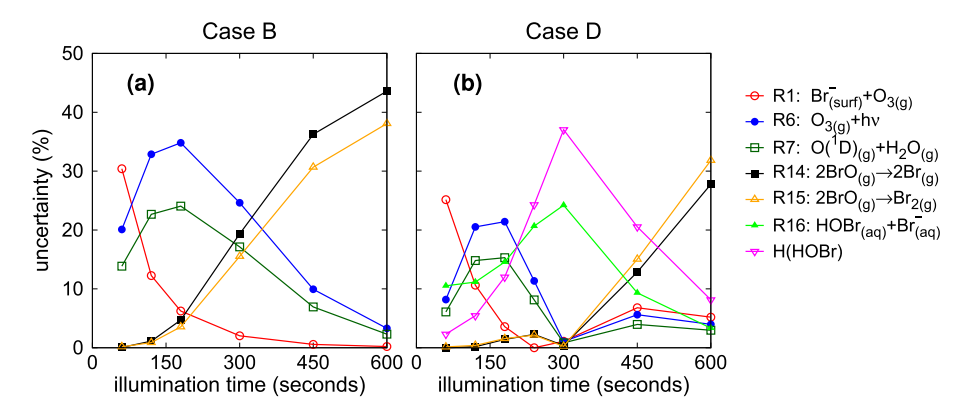


Fig. 6. Input parameters' contribution to the uncertainty in MAGIC's predictions of $Br_{2(g)}$ levels for (a) case B and (b) case D. Input parameters that contribute at least 15% to the uncertainty in $[Br_{2(g)}]$ for at least one analysis time are shown in the figure. Reaction rate constants are represented by R followed by the chemical reaction number from the text. H(HOBr) represents the Henry's law constant for HOBr.

Na⁺/Br⁻ ratio as in sea water (Gabriel et al., 2002). Aerosol size distribution, pH, and RH are calculated or chosen to be typical of the remote MBL.

In the MBL case simulations, the system is kept in the dark for 50 min then exposed to sunlight for six hours. Photolysis rate constants are calculated using published absorption cross sections (Sander et al., 2011) and actinic fluxes reported in Finlayson-Pitts et al. (2000) for a location at 30°N latitude on July 1. The intensity of the actinic flux increases slowly during the sunlight period to simulate sunrise at a solar zenith angle of 86° ($\sim 5:30$ am) to 10° ($\sim 11:30$ am). During the entire simulation the temperature is held constant at 298 K. As in cases A-D, the MBL case assumes that the total aerosol surface area and volume in the system is constant during the simulations. Although larger aerosols are rapidly removed from the atmosphere due to deposition in the real marine boundary layer, dry deposition residence times for micronsized particles can be quite long (\sim 5 h for 10 μ m sea-salt aerosols at 10 m s⁻¹ wind speeds, Lewis and Schwartz, 2004). Unlike cases A-D, the MBL case does not consider irreversible losses of gas-phase species due to wall losses or dilution of the chamber contents.

Fig. 7 shows that brominated species are produced much more rapidly during the sunlight period than during the initial dark period in the MBL case, although in smaller quantities than observed in cases A–D due to much lower $[O_{3(g)}]_0$ and $[Br^-_{(aq)}]_0$ (Table 1). Both $[HOBr_{(g)}]$ and $[Br_{2(g)}]$ have similar temporal trends during the sunlight period and their sum is plotted versus time in Fig. 7a. Unlike cases A–D where most bromine atoms are converted to $Br_{2(g)}$, levels of $Br_{2(g)}$ are approximately two orders of magnitude smaller than either $HOBr_{(g)}$ or $BrO_{(g)}$ during the sunlight period in the MBL case due to enhanced photolysis of $Br_{2(g)}$ in the actinic region (discussed below).

Although the MBL case excludes chlorine, iodine, and NO_X chemistry, it is interesting to note that the peak concentrations of brominated species in the MBL case are comparable with those reported in the literature for clean, mid-latitude marine boundary layers. Leser et al. (2003) measured a maximum daytime BrO concentration of 2.4 ppt over the Atlantic Ocean during October. Saiz-Lopez et al. (2004) measured an average daytime BrO concentration of 2.3 ppt during August at Mace Head Observatory, Ireland, with a peak concentration of 6.5 ppt. Although the MBL case simulations predict higher peak $BrO_{(g)}$ levels (\sim 16 ppt, Fig. 7b), this may be due in part to the MBL case simulations using an actinic flux typical of July; photolysis of ozone produces HO_X radicals, initiating the bromine explosion pathway. Higher rates of photolysis ultimately lead to higher concentrations of brominated species such as BrO.

Measurements of BrO also are available in clean, low-latitude air masses. Read et al. (2008) report an average daytime peak BrO concentration of 2.5 ppt at Cape Verde Observatory during November to June, and Martin et al. (2009) report a maximum BrO concentration of 10.2 ppt off the West African coast during February.

There are fewer studies that report Br_2 concentrations in the mid-latitude MBL. Finley and Saltzman (2008) measured Br_2 levels on the coast of Southern California during January, observing mean Br_2 levels of 2.3 ppt. In the MBL simulations, peak Br_2 levels are lower (~ 0.15 pptv), due in part to the MBL case simulations using an actinic flux typical of July; photolysis is the main destruction pathway of Br_2 in the MBL case.

Ozone levels (Fig. 7c) drop by 20% (20 ppbv—16 ppbv) during the six hours of sunlight in the MBL case, with one-third of the ozone destruction due to reaction with brominated species. Similar rates of ozone loss during the morning are reported in the remote marine boundary layer (Dickerson et al., 1999; Nagao et al., 1999; Galbally et al., 2000) and halogen reactions are hypothesized to account for a significant fraction of the observed ozone destruction.

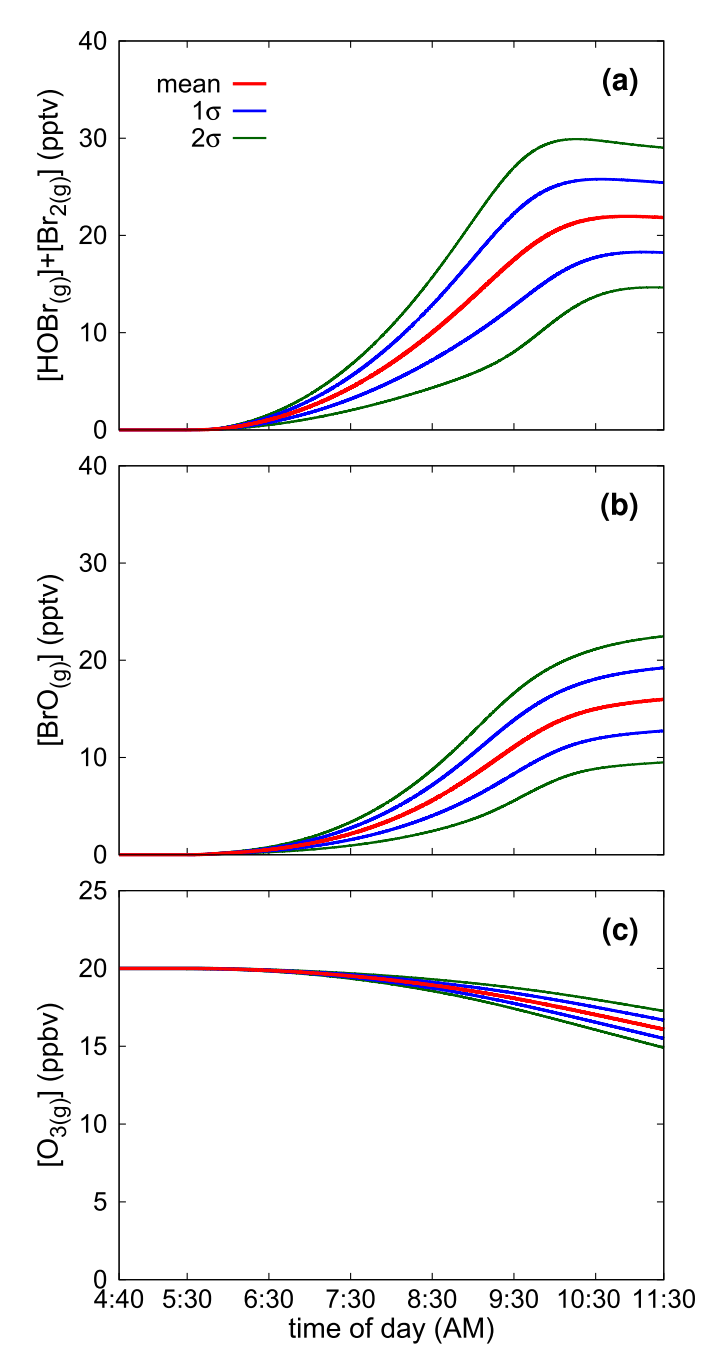


Fig. 7. Results from the MAGIC model for the MBL case. The mean, 1σ , and 2σ lines are based on the 5000 simulations from the sensitivity analysis performed on MAGIC. Sunrise begins at 5:30 am.

The concentration of bromide declines to 10% of its initial value by $\sim\!9:50$ am, indicating the system is bromide-limited. For this reason, the results of the sensitivity study conducted on the MBL case are compared with the sensitivity study conducted on case D, which is bromide-limited as well. However, many of the mechanisms in $Br_{2(g)}$ production for the MBL case are different from case D. During the initial dark period, interfacial reaction (1) creates only $\sim\!20\%$ of $Br_{2(g)}$ in the MBL case and most $Br_{2(g)}$ is produced through the following mechanism during the first 50 min of the simulation: $O_{3(g)}$ dissolves into the aerosols and reacts with bromide to produce $BrO^-_{(aq)}$, which protonates to form $HOBr_{(aq)}$. Aqueous Br_2 is created when $HOBr_{(aq)}$ reacts with $Br^-_{(aq)}$ via reaction (16) and its acidic form,

$$HOBr_{(aq)} + Br_{(aq)}^{-} + H_{(aq)}^{+} \rightarrow Br_{2(aq)} + H_{2}O_{(aq)}.$$
 (20)

The acid-catalyzed reaction (20) has been proposed as being key for bromide activation in polar regions (Grannas et al., 2007; Simpson et al., 2007; Piot and von Glasow, 2008) and midlatitudes (Sander and Crutzen, 1996; Vogt et al., 1996; Fickert et al., 1999; Sander et al., 2003; Smoydzin and von Glasow, 2009), but produces an insignificant amount of $Br_{2(aq)}$ in cases A–D because OH⁻ formation via reaction (16) results in an aerosol pH of \sim 11. However, low aerosol pH results in reaction (20) dominating $Br_{2(aq)}$ production in the MBL case.

Prior to bromide depletion in both case D (Fig. 2) and the MBL case (Fig. 8), bromine production is quite sensitive to ozone photolysis (reaction 6), OH formation via reaction (7), and $O(^1D)$ quenching with N_2 via reaction (8). However, many of the key chemical and physical processes in the production of $Br_{2(g)}$ differ between the two cases. In case D, the bromine explosion mechanism, which relies on the rapid production of gaseous HOBr (see Section 3.2.1) dominates $Br_{2(g)}$ production. During the first hour of sunlight in the MBL case, $HOBr_{(g)}$ levels are relatively low and the majority of $Br_{2(aq)}$ is produced slowly through the following mechanism,

$$Br_{(aq)}^{-} + OH_{(aq)} \rightarrow HOBr_{(aq)}^{-}, \tag{21}$$

$$HOBr_{(aq)}^{-} + Br_{(aq)}^{-} \rightarrow Br_{2(aq)}^{-} + OH_{(aq)}^{-},$$
 (22)

$$Br_{2(aq)}^{-} + HO_{2(aq)} \rightarrow Br_{2(aq)} + HO_{2(aq)}^{-},$$
 (23)

with most aqueous OH and HO_2 radicals originating in the gasphase. As the simulations progress and more Br_2 is released from the aerosols, $HOBr_{(g)}$ levels increase and reaction (20) of $HOBr_{(aq)}$ with $Br_{(aq)}^-$ overtakes reaction (23) as the major source of aqueous bromine. The growing importance of HOBr in the production of bromine is reflected in the increasing regression coefficient for reaction (20).

The main sources and sinks of many key species are different in the MBL case compared to case D. In the MBL case, $HOBr_{(g)}$, $Br_{2(g)}$, and $BrO_{(g)}$ are primarily destroyed through photolysis,

$$HOBr_{(g)} + h\nu \rightarrow OH_{(g)} + Br_{(g)}, \tag{24}$$

$$Br_{2(g)} + h\nu \rightarrow 2 Br_{(g)},$$
 (25)

$$BrO_{(g)} + h\nu \rightarrow Br_{(g)} + O(^{3}P),$$
 (26)

due to their large absorption cross sections in the actinic region, and gaseous bromine levels are most sensitive to $Br_{2(g)}$ photolysis throughout the simulation. Photolysis, along with reactions involving HO_X radicals, also is the dominant destruction pathway of ozone in the MBL case instead of reaction (13) with atomic bromine as in case D. Although HOBr is critical in the release of bromine in both case D and the MBL case, the main source of HOBr shifts from reaction (11) of $OH_{(g)}$ with $Br_{2(g)}$ in case D to reaction (12) of $HO_{2(g)}$ with $Br_{2(g)}$ in the MBL case.

After approximately 4.5 h of sunlight the aerosols become depleted of bromide (<10% of the initial concentration by 9:50 am), resulting in the termination of Br $_2$ production in the aqueousphase. At this time, most of the bromine atoms are stored in HOBr $_{(g)}$ and BrO $_{(g)}$, whose concentrations are two orders of magnitude greater than the concentration of Br $_{2(g)}$. Gaseous bromine is formed primarily via the BrO $_{(g)}$ self-reaction (15) throughout the remainder of the simulation. This shift in Br $_{2(g)}$

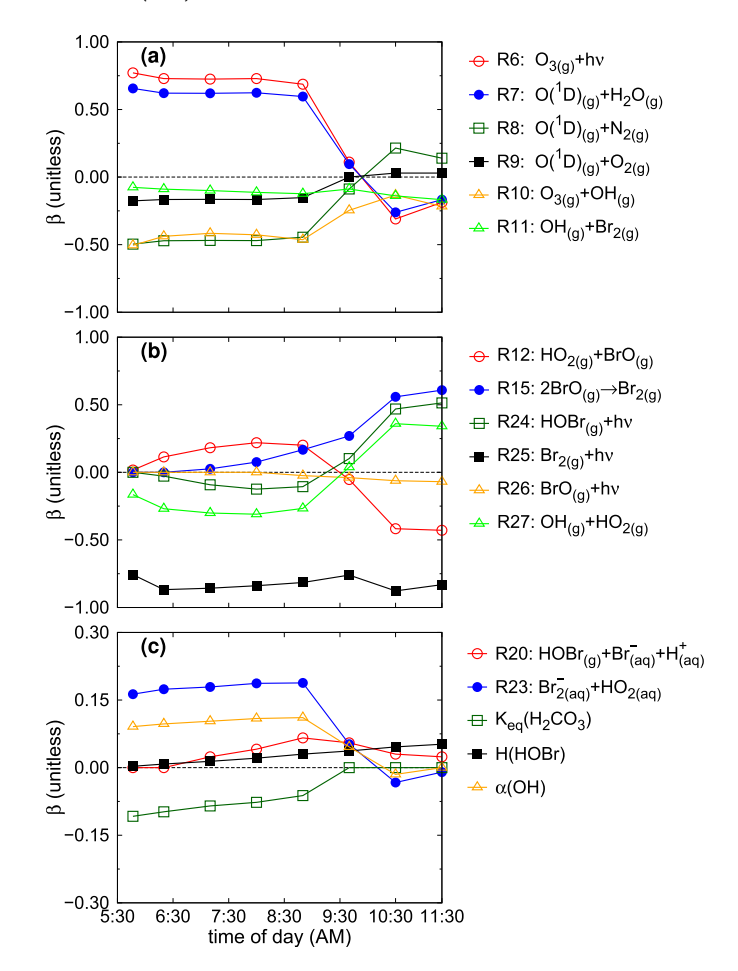


Fig. 8. Sensitivity of $[Br_{2(g)}]$ to input parameters at various times during the morning hours for the MBL case. The input parameters are significant at the 0.05 level and have either a regression coefficient greater than 0.2 for at least one analysis time or are deemed interesting by the authors. Sunrise begins at 5:30 am. Reaction rate constants are represented by R followed by the chemical reaction number from the text. $K_{eq}(X)$, H(X), and $\alpha(X)$ represent the acid—base equilibrium constant, Henry's law constant, and mass accommodation coefficient of species X, respectively.

production mechanisms greatly affects the regression coefficients of many input parameters.

Prior to bromide depletion, $HOBr_{(g)}$ formation via reaction (12) of $HO_{2(g)}$ and $BrO_{(g)}$ is positively correlated with $Br_{2(g)}$ levels since that reaction increases the amount of aqueous HOBr available to produce $Br_{2(aq)}$ via reactions (16) and (20) with $Br_{(aq)}^-$. Ozone photolysis and reaction (7) of $O(^1D)$ with H_2O indirectly increase $HOBr_{(g)}$ production by initiating HO_x formation, resulting in positive regression coefficients for these reactions. Photolysis of $HOBr_{(g)}$ is negatively correlated with bromine formation, as are reactions that reduce HO_x levels such as the $O(^1D)_{(g)}$ quenching reactions (8) and (9), and reaction (27),

$$OH_{(g)} + HO_{2(g)} \rightarrow O_{2(g)} + H_2O_{(g)}.$$
 (27)

The processes with the highest regression coefficients at peak $[Br_{2(g)}]$ in the MBL case are summarized in Fig. 5b.

At the onset of bromide depletion, the main source of $Br_{2(g)}$ is the liberation of bromine atoms from $HOBr_{(g)}$. As a result, the regression coefficients of reactions (6–9), (12), (24), and (27) change sign. Photolysis of $HOBr_{(g)}$ now has a positive regression coefficient since it liberates bromine atoms which are able to form $BrO_{(g)}$ via reaction (13) with $O_{3(g)}$. The $BrO_{(g)}$ self-reaction (15) begins to dominate gaseous bromine production and has a positive

regression coefficient, while HOBr(g) formation via reaction (12) of $HO_{2(g)}$ and $BrO_{(g)}$ becomes negatively correlated with $Br_{2(g)}$ levels since that reaction reduces BrO_(g) levels.

While the MBL simulation does not account for meteorology, the amount of time from sunrise to bromide depletion is approximately the same amount of time required for dry deposition of the largest aerosols in the simulation (10 μm). After depletion, $Br_{2(g)}$ formation can continue through $BrO_{(g)}$ self-reaction (15).

Bromide depletion in the aerosols also has a large impact on the sources of uncertainty for the MBL case (Supplementary Fig. 4). At all times during the illumination period, $Br_{2(g)}$ photolysis is responsible for ~30-60% of the total uncertainty since this reaction is the major $Br_{2(g)}$ loss pathway. During the first four hours of sunlight, about half of the model uncertainty is generated by ozone photolysis, reaction (7) of $O(^{1}D)$ with $H_{2}O$, reaction (10) of $O_{3(g)}$ with $OH_{(g)}$, and the mass accommodation coefficient of OH, all of which impact HO_x levels. Following bromide depletion, those four input parameters produce negligible uncertainty and the BrO(g) self-reaction (15) and HOBr(g) photolysis generate about half of the uncertainty since they determine the rate of liberation of bromine atoms from the BrO_(g) and HOBr_(g) reservoirs.

4. Summary

This study illustrates the strength of applying a detailed kinetics treatment of a chemical mechanism to experimental data in identifying the most important processes in the mechanism and how they vary with time. Rapid bromine formation from NaBr aerosols is reported in chamber experiments (cases A–D) and mechanisms are tracked for the liberation of aqueous bromide into gaseous Br₂ under different experimental conditions based on sensitivity studies conducted on the MAGIC model. As in the recent work of Buxmann et al. (2012) using deliquesced samples of NaCl/NaBr, the bromine "explosion" observed in polar regions is replicated in chamber experiments but in the present case, using pure, deliquesced NaBr aerosols. The mechanism consists of (1) production of HOBr in the gas-phase, (2) uptake of HOBr into the aqueous-phase, (3) reaction of $HOBr_{(aq)}$ with $Br_{(aq)}^{-}$ to produce $Br_{2(aq)}$, and (4) degassing of Br_{2(aq)} from the aerosols. Although the heterogeneous reaction of O_{3(g)} with interfacial Br⁻ is important in the dark, both interface OH and O₃ reactions are too slow to produce a substantial amount of Br_{2(g)} during the UV period. Gaseous bromine is generated as long as there are ample ozone and bromide in the system. If ozone is depleted first, the peak [Br_{2(g)}] is most sensitive to gasphase reactions and these reactions are responsible for most of the model uncertainty. In particular, O3-limited systems are increasingly sensitive to competition between the two BrO selfreactions (reactions 14 and 15). However, when the system is bromide-limited, peak [Br_{2(g)}] becomes sensitive to aqueous-phase reactions and mass transfer parameters, and most of the model uncertainty comes from these processes. Br_{2(g)} output also is sensitive to aerosol size distributions in this regime.

A separate set of simulations is conducted using initial conditions similar to the remote marine boundary layer (MBL case). In this case, bromide is liberated from aerosols through the same four steps as in cases A–D, but with different reactions playing key roles. While interhalogen and nitrogen oxide chemistry are not included in the MBL case, it is notable that the predicted levels of active bromine species are comparable with marine boundary layer measurements in low- and mid-latitude regions (Leser et al., 2003; Saiz-Lopez et al., 2004; Read et al., 2008; Martin et al., 2009; Saiz-Lopez and von Glasow, 2012). Bromine production in the MBL case is bromide-limited and the sensitivity of Br2(g) levels to input parameters change dramatically once bromide is depleted from the aerosols. After bromide depletion, Br_{2(g)} formation continues via

gaseous BrO reactions. This work demonstrates that sources of uncertainty in modeling studies can vary greatly in time, especially when the depletion of key reactants occurs. Physical and chemical processes may alternate between aiding and hindering the formation of chemical species, depending on the current conditions in the system. In the MBL case, the input parameters that produce the greatest amount of model uncertainty are gas-phase reactions whose uncertainty ranges are relatively well-established (Supplementary Fig. 4). However, simulations indicate that special attention should be given to modeling the photolysis conditions and aerosol properties as accurately as possible since both may strongly influence the timing or occurrence of depletion in the remote marine boundary layer.

Acknowledgments

The authors would like to thank Lee-Huang Chen for his assistance in processing and organizing data from the sensitivity and uncertainty analyses. This work was funded in part by the National Science Foundation (NSF Grant CHE-0909227) and the Department of Energy (DOE Grant ER62578). We are grateful to James N. Pitts Jr. for helpful discussions and comments on the manuscript.

Appendix A. Supplementary data

Supplementary data related to this article can be found at http:// dx.doi.org/10.1016/j.atmosenv.2014.02.056.

References

Abbatt, J., Oldridge, N., Symington, A., Chukalovskiy, V., McWhinney, R.D., Sjostedt, S., Cox, R.A., 2010. Release of gas-phase halogens by photolytic generation of OH in frozen halide-nitrate solutions: an active halogen formation mechanism? The Journal of Physical Chemistry A 114, 6527-6533.

Abbatt, J.P.D., 1994. Heterogeneous reaction of HOBr with HBr and HCl on ice surfaces at 228 K. Geophysical Research Letters 21, 665-668.

Abbatt, J.P.D., Waschewsky, G.C.G., 1998. Heterogeneous interactions of HOBr, HNO₃, O₃, and NO₂ with deliquescent NaCl aerosols at room temperature. Journal of Physical Chemistry A 102, 3719-3725.

Abbatt, J.P.D., Thomas, J.L., Abrahamsson, K., Boxe, C., Granfors, A., Jones, A.E., King, M.D., Saiz-Lopez, A., Shepson, P.B., Sodeau, J., Toohey, D.W., Toubin, C., von Glasow, R., Wren, S.N., Yang, X., 2012. Halogen activation via interactions with environmental ice and snow in the polar lower troposphere and other regions. Atmospheric Chemistry and Physics 12, 6237-6271.

Allanic, A., Oppliger, R., Rossi, M.J., 1997. Real-time kinetics of the uptake of HOBr and BrONO2 on ice and in the presence of HCl in the temperature range 190-200 K. Journal of Geophysical Research: Atmospheres 102, 23529–23541.

Anastasio, C., Mozurkewich, M., 2002. Laboratory studies of bromide oxidation in the presence of ozone; evidence for a glass-surface mediated reaction, Journal of Atmospheric Chemistry 41, 135–162. Archer, C.L., Jacobson, M.Z., 2005. Evaluation of global wind power. Journal of

Geophysical Research 110, D12110.

Ayers, G.P., Cainey, J.M., Granek, H., Leck, C., 1996. Dimethylsulfide oxidation and the ratio of methanesulfonate to non sea-salt sulfate. Journal of Atmospheric Chemistry 25, 307-325.

Barrie, L., Platt, U., 1997. Arctic tropospheric chemistry: an overview. Tellus B 49, 450-454

Barrie, L.A., Bottenheim, J.W., Schnell, R.C., Crutzen, P.J., Rasmussen, R.A., 1988. Ozone destruction and photochemical reactions at polar sunrise in the lower arctic atmosphere. Nature 334, 138-141.

Behnke, W., Elend, M., Krüger, U., Zetzsch, C., 1999. The influence of NaBr/NaCl ratio on the Br-catalysed production of halogenated radicals. Journal of Atmospheric Chemistry 34, 87-99.

Berko, H.N., McCaslin, P.C., Finlayson-Pitts, B.J., 1991. Formation of gas-phase bromine compounds by reaction of solid NaBr with gaseous ClONO2, Cl2, and BrCl at 298 K. Journal of Physical Chemistry 95, 6951-6958.

Bertram, A.K., Ivanov, A.V., Hunter, M., Molina, L.T., Molina, M.J., 2001. The reaction probability of OH on organic surfaces of tropospheric interest. Journal of Physical Chemistry A 105, 9415–9421.

Boodaghians, R.B., Hall, I.W., Wayne, R.P., 1987. Kinetics of the reactions of the hydroxyl radical with molecular chlorine and bromine. Journal of the Chemical Society, Faraday Transactions 2 (83), 529-538.

Bottenheim, J.W., Dibb, J.E., Honrath, R.E., Shepson, P.B., 2002. An introduction to the ALERT 2000 and SUMMIT 2000 Arctic research studies. Atmospheric Environment 36, 2467-2469.

- Burrows, J.P., Wallington, T.J., Wayne, R.P., 1984. Kinetics of the reaction of OH with ClO. Journal of the Chemical Society, Faraday Transactions 2 (80), 957–971.
- Buxmann, J., Balzer, N., Bleicher, S., Platt, U., Zetzsch, C., 2012. Observations of bromine explosions in smog chamber experiments above a model salt Pan. International Journal of Chemical Kinetics 44, 312–326.
- Chu, L., Chu, L.T., 1999. Heterogeneous interaction and reaction of HOBr on ice films. The Journal of Physical Chemistry A 103, 8640–8649.
- Clifford, D., Donaldson, D.J., 2007. Direct experimental evidence for a heterogeneous reaction of ozone with bromide at the air—aqueous interface. The Journal of Physical Chemistry A 111, 9809—9814.
- DeHaan, D.O., Brauers, T., Oum, K., Stutz, J., Nordmeyer, T., Finlayson-Pitts, B.J., 1999. Heterogeneous chemistry in the troposphere: experimental approaches and applications to the chemistry of sea salt particles. International Reviews in Physical Chemistry 18, 343–385.
- Derwent, R., Høv, O., 1988. Application of sensitivity and uncertainty analysis techniques to a photochemical ozone model. Journal of Geophysical Research 93, 5185–5199.
- Dickerson, R.R., Rhoads, K.P., Carsey, T.P., Oltmans, S.J., Burrows, J.P., Crutzen, P.J., 1999. Ozone in the remote marine boundary layer: a possible role for halogens. Journal of Geophysical Research 104, 21385—21395.
- Fan, S., Jacob, D.J., 1992. Surface ozone depletion in Arctic spring sustained by bromine reactions on aerosols. Nature 359, 522–524.
- Fickert, S., Adams, J.W., Crowley, J.N., 1999. Activation of Br₂ and BrCl via uptake of HOBr onto aqueous salt solutions. Journal of Geophysical Research 104, 23719—23727.
- Finlayson-Pitts, B.J., Johnson, S.N., 1988. The reaction of NO₂ with NaBr: possible source of BrNO in polluted marine atmospheres. Atmospheric Environment 22, 1107—1112.
- Finlayson-Pitts, B.J., Livingston, F.E., Berko, H.N., 1990. Ozone destruction and bromine photochemistry at ground level in the Arctic spring. Nature 343, 622–625.
- Finlayson-Pitts, B.J., Ezell, M.J., Jayaweera, T.M., Berko, H.N., Lai, C.C., 1992. Kinetics of the reactions of OH with methyl chloroform and methane: implications for global tropospheric OH and the methane budget. Geophysical Research Letters 19, 1371–1374.
- Finlayson-Pitts, B.J., Pitts Jr., J.N., 2000. Chemistry of the Upper and Lower Atmosphere Theory, Experiments, and Applications. Academic Press, San Diego.
- Finley, B.D., Saltzman, E.S., 2008. Observations of Cl₂, Br₂, and I₂ in coastal marine air. Journal of Geophysical Research: Atmospheres 113, D21301.
- Foster, K.L., Plastridge, R.A., Bottenheim, J.W., Shepson, P.B., Finlayson-Pitts, B.J., Spicer, C.W., 2001. The role of Br₂ and BrCl in surface ozone destruction at polar sunrise. Science 291, 471–474.
- Fridlind, A.M., Jacobson, M.Z., 2000. A study of gas-aerosol equilibrium and aerosol pH in the remote marine boundary layer during the First Aerosol Characterization Experiment (ACE 1). Journal of Geophysical Research 105, 17325–17340.
- Frinak, E.K., Abbatt, J.P.D., 2006. Br₂ production from the heterogeneous reaction of Gas-Phase OH with aqueous salt Solutions: impacts of acidity, halide concentration, and organic surfactants. The Journal of Physical Chemistry A 110, 10456—10464.
- Gabriel, R., von Glasow, R., Sander, R., Andreae, M.O., Crutzen, P.J., 2002. Bromide content of sea-salt aerosol particles collected over the Indian Ocean during INDOEX 1999. Journal of Geophysical Research 107, 8032.
- Galbally, I.E., Bentley, S.T., Meyer, C.P., 2000. Mid-latitude marine boundary-layer ozone destruction at visible sunrise observed at Cape Grim, Tasmania, 41°S. Geophysical Research Letters 27, 3841–3844.
- Ganske, J.A., Ezell, M.J., Berko, H.N., Finlayson-Pitts, B.J., 1991. The reaction of OH with ClNO₂ at 298 K: kinetics and mechanisms. Chemical Physics Letters 179, 204–210.
- Ganske, J.A., Berko, H.N., Ezell, M.J., Finlayson-Pitts, B.J., 1992. Kinetics of the gasphase reaction of OH with ClNO₂ from 259 to 348 K. Journal of Physical Chemistry 96, 2568–2572.
- Gao, D.F., Stockwell, W.R., Milford, J.B., 1995. First-order sensitivity and uncertainty analysis for a regional-scale gas-phase chemical mechanism. Journal of Geophysical Research 100, 23153—23166.
- Gao, D.F., Stockwell, W.R., Milford, J.B., 1996. Global uncertainty analysis of a regional-scale gas-phase chemical mechanism. Journal of Geophysical Research 101, 9107—9119.
- George, I.J., Anastasio, C., 2007. Release of gaseous bromine from the photolysis of nitrate and hydrogen peroxide in simulated sea-salt solutions. Atmospheric Environment 41, 543–553.
- Ghosal, S., Hemminger, J.C., Bluhm, H., Mun, B.S., Hebenstreit, E., Ketteler, G., Ogletree, F., Requejo, F., Salmeron, M., 2005. Electron spectroscopy of aqueous solution interfaces reveals surface enhancement of halides: implications for atmospheric chemistry. Science 307, 563–566.
- Gomer, T., Brauers, T., Heintz, T., Stutz, J., Platt, U., 1995. MFC Manual Version 1.99. Grannas, A.M., Jones, A.E., Dibb, J., Ammann, M., Anastasio, C., Beine, H.J., Bergin, M., Bottenheim, J., Boxe, C.S., Carver, G., Chen, G., Crawford, J.H., Domine, F., Frey, M.M., Guzman, M.I., Heard, D.E., Helmig, D., Hoffmann, M.R., Honrath, R.E., Huey, L.G., Hutterli, M., Jacobi, H.W., Klan, P., Lefer, B., McConnell, J., Plane, J., Sander, R., Savarino, J., Shepson, P.B., Simpson, W.R., Sodeau, J.R., von Glasow, R., Weller, R., Wolff, E.W., Zhu, T., 2007. An overview of snow photochemistry: evidence, mechanisms and impacts. Atmospheric Chemistry and Physics 7, 4329–4373.
- Guzman, M.I., Athalye, R.R., Rodriguez, J.M., 2012. Concentration effects and ion properties controlling the fractionation of halides during aerosol formation. The Journal of Physical Chemistry A 116, 5428–5435.

- Hausmann, M., Platt, U., 1994. Spectroscopic measurement of bromine oxide and ozone in the high Arctic during Polar Sunrise Experiment 1992. Journal of Geophysical Research: Atmospheres 99, 25399—25413.
- Hebestreit, K., Stutz, J., Rosen, D., Matviev, V., Peleg, M., Luria, M., Platt, U., 1999. DOAS measurements of tropospheric bromine oxide in mid-latitudes. Science 283, 55–57.
- Hirokawa, J., Onaka, K., Kajii, Y., Akimoto, H., 1998. Heterogeneous processes involving sodium halide particles and ozone: molecular bromine release in the marine boundary layer in the absence of nitrogen oxides. Geophysical Research Letters 25, 2449–2452.
- Hönninger, G., Bobrowski, K., Palenque, E.R., Torrez, R., Platt, U., 2004. Reactive bromine and sulfur emissions at Salar de Uyuni, Bolivia. Geophysical Research Letters 31, L04101.
- Hsu, Y.-C., Chen, D.-S., Lee, Y.-P., 1987. Rate constant for the reaction of OH radicals with dimethyl sulfide. International Journal of Chemical Kinetics 19, 1073—1082.
- Hunt, S.W., Roeselová, M., Wang, W., Wingen, L.M., Knipping, E.M., Tobias, D.J., Dabdub, D., Finlayson-Pitts, B.J., 2004. Formation of molecular bromine from the reaction of ozone with deliquesced NaBr aerosol: evidence for interface chemistry. Journal of Physical Chemistry A 108, 11559—11572.
- Jungwirth, P., Tobias, D.J., 2001. Molecular structure of salt solutions: a new view of the interface with implications for heterogeneous atmospheric chemistry. Journal of Physical Chemistry B 105, 10468–10472.
- Jungwirth, P., Tobias, D.J., 2002. Ions at the air/water interface. Journal of Physical Chemistry B 106, 6361–6373.
- Keene, W.C., Sander, R., Pszenny, A.A.P., Vogt, R., Crutzen, P.J., Galloway, J.N., 1998. Aerosol pH in the marine boundary layer: a review and model evaluation. Journal of Aerosol Science 29, 339–356.
- Kirchner, U., Benter, T., Schindler, R.N., 1997. Experimental verification of gas phase bromine enrichment in reactions of HOBr with sea salt doped ice surfaces. Berichte der Bunsengesellschaft für Physikalische Chemie 101, 975–977.
- Knipping, E.M., Lakin, M.J., Foster, K.L., Jungwirth, P., Tobias, D.J., Gerber, R.B., Dabdub, D., Finlayson-Pitts, B.J., 2000. Experiments and simulations of ionenhanced interfacial chemistry on aqueous NaCl aerosols. Science 288, 301–306.
- Knipping, E.M., Dabdub, D., 2002. Modeling Cl₂ formation from aqueous NaCl particles: evidence for interfacial reactions and importance of Cl₂ decomposition in alkaline solution. Journal of Geophysical Research 107, 4360–4389.
- Laskin, A., Wang, H., Robertson, W.H., Cowin, J.P., Ezell, M.J., Finlayson-Pitts, B.J., 2006. A new approach to determining gas-particle reaction probabilities and application to the heterogeneous reaction of deliquesced sodium chloride particles with gas-phase hydroxyl radicals. Journal of Physical Chemistry A 110, 10619–10627.
- Leser, H., Hönninger, G., Platt, U., 2003. MAX-DOAS measurements of BrO and NO₂ in the marine boundary layer. Geophysical Research Letters 30, 1537.
- Lewis, E.R., Schwartz, S.E., 2004. Sea Salt Aerosol Production: Mechanisms, Methods, Measurements, and Models a Critical Review. American Geophysical Union, Washington, D. C.
- Liao, J., Huey, L.G., Tanner, D.J., Flocke, F.M., Orlando, J.J., Neuman, J.A., Nowak, J.B., Weinheimer, A.J., Hall, S.R., Smith, J.N., Fried, A., Staebler, R.M., Wang, Y., Koo, J.H., Cantrell, C.A., Weibring, P., Walega, J., Knapp, D.J., Shepson, P.B., Stephens, C.R., 2012. Observations of inorganic bromine (HOBr, BrO, and Br₂) speciation at Barrow, Alaska, in spring 2009. Journal of Geophysical Research: Atmospheres 117, D00R16.
- Liu, Q., Schurter, L.M., Muller, C.E., Aloisio, S., Francisco, J.S., Margerum, D.W., 2001. Kinetics and mechanisms of aqueous ozone reactions with bromide, sulfite, hydrogen sulfite, iodide, and nitrite ions. Inorganic Chemistry 40, 4436–4442.
- Martin, M., Pöhler, D., Seitz, K., Sinreich, R., Platt, U., 2009. BrO measurements over the Eastern North-Atlantic. Atmospheric Chemistry and Physics 9, 9545–9554.
- Matveev, V., Peleg, M., Rosen, D., Tov-Alper, D.S., Hebestreit, K., Stutz, J., Platt, U., Blake, D., Luria, M., 2001. Bromine oxide ozone interaction over the Dead Sea. Journal of Geophysical Research 106, 10375—10387.
- McKay, M.D., Beckman, R.J., Conover, W.J., 1979. Comparison of three methods for selecting values of input variables in the analysis of output from a computer code. Technometrics 21, 239–245.
- Mochida, M., Akimoto, H., vanDenBergh, H., Rossi, M.J., 1998. Heterogeneous kinetics of the uptake of HOBr on solid alkali metal halides at ambient temperature. Journal of Physical Chemistry A 102, 4819–4828.
- Nagao, I., Matsumoto, K., Tanaka, H., 1999. Sunrise ozone destruction found in the sub-tropical marine boundary layer. Geophysical Research Letters 26, 3377–3380.
- Nissenson, P., Thomas, J.L., Finlayson-Pitts, B.J., Dabdub, D., 2008. Sensitivity and uncertainty analysis of the mechanism of gas-phase chlorine production from NaCl aerosols in the MAGIC model. Atmospheric Environment 43, 6934–6941.
- Nissenson, P., Packwood, D.M., Hunt, S.W., Finlayson-Pitts, B.J., Dabdub, D., 2009. Probing the sensitivity of gaseous Br₂ production from the oxidation of aqueous bromide-containing aerosols and atmospheric implications. Atmospheric Environment 43, 3951–3962.
- O'Dowd, C.D., Smith, M.H., Consterdine, I.E., Lowe, J.A., 1997. Marine aerosol, seasalt, and the marine sulphur cycle: a short review. Atmospheric Environment 31, 73–80.
- Oldridge, N.W., Abbatt, J.P.D., 2011. Formation of gas-phase bromine from interaction of ozone with frozen and liquid NaCl/NaBr solutions: quantitative separation of surficial chemistry from bulk-phase reaction. The Journal of Physical Chemistry A 115, 2590–2598.
- Oum, K.W., Lakin, M.J., DeHaan, D.O., Brauers, T., Finlayson-Pitts, B.J., 1998a. Formation of molecular chlorine from the photolysis of ozone and aqueous sea-salt particles. Science 279, 74–77.

- Oum, K.W., Lakin, M.J., Finlayson-Pitts, B.J., 1998b. Bromine activation in the troposphere by the dark reaction of O₃ with seawater ice. Geophysical Research Letters 25, 3923–3926.
- Piot, M., von Glasow, R., 2008. The potential importance of frost flowers, recycling on snow, and open leads for ozone depletion events. Atmospheric Chemistry and Physics 8, 2437–2467.
- Platt, U., Stutz, J., 1998. Differential Optical Absorption Spectroscopy: Principles and Applications. Springer-Verlag, Berlin Heidelberg.
- Pratt, K.A., Custard, K.D., Shepson, P.B., Douglas, T.A., Pohler, D., General, S., Zielcke, J., Simpson, W.R., Platt, U., Tanner, D.J., Gregory Huey, L., Carlsen, M., Stirm, B.H., 2013. Photochemical production of molecular bromine in Arctic surface snowpacks. Nature Geoscience 6, 351–356.
- Pszenny, A.A.P., Moldanov, J., Keene, W.C., Sander, R., Maben, J.R., Martinez, M., Crutzen, P.J., Perner, D., Prinn, R.G., 2004. Halogen cycling and aerosol pH in the Hawaiian marine boundary layer. Atmospheric Chemistry and Physics 4, 147–168.
- Read, K.A., Mahajan, A.S., Carpenter, L.J., Evans, M.J., Faria, B.V.E., Heard, D.E., Hopkins, J.R., Lee, J.D., Moller, S.J., Lewis, A.C., Mendes, L., McQuaid, J.B., Oetjen, H., Saiz-Lopez, A., Pilling, M.J., Plane, J.M.C., 2008. Extensive halogenmediated ozone destruction over the tropical Atlantic Ocean. Nature 453, 1232—1235.
- Richards-Henderson, N.K., Callahan, K.M., Nissenson, P., Nishino, N., Tobias, D.J., Finlayson-Pitts, B.J., 2013. Production of gas phase NO₂ and halogens from the photolysis of thin water films containing nitrate, chloride and bromide ions at room temperature. Physical Chemistry Chemical Physics 15, 17636—17646.
- Richards, N.K., Finlayson-Pitts, B.J., 2012. Production of gas phase NO₂ and halogens from the photochemical oxidation of aqueous mixtures of sea salt and nitrate ions at room temperature. Environmental Science & Technology 46, 10447—10454
- Rodriguez, M.A., Dabdub, D., 2003. Monte Carlo uncertainty and sensitivity analysis of the CACM chemical mechanism. Journal of Geophysical Research 108, 4443—4451.
- Saiz-Lopez, A., Plane, J.M.C., Shillito, J.A., 2004. Bromine oxide in the mid-latitude marine boundary layer. Geophysical Research Letters 31, L03111.
- Saiz-Lopez, A., von Glasow, R., 2012. Reactive halogen chemistry in the troposphere. Chemical Society Reviews 41, 6448–6472.
- Sander, R., Crutzen, P.J., 1996. Model study indicating halogen activation and ozone destruction in polluted air masses transported to the sea. Journal of Geophysical Research 101, 9121–9138.
- Sander, R., Keene, W.C., Pszenny, A.A.P., Arimoto, R., Ayers, G.P., Baboukas, E., Cainey, J.M., Crutzen, P.J., Duce, R.A., Hönninger, G., Huebert, B.J., Maenhaut, W., Mihalopoulos, N., Turekian, V.C., Dingenen, R.V., 2003. Inorganic bromine in the marine boundary layer: a critical review. Atmospheric Chemistry and Physics Discussions 3, 2963–3050.
- Sander, S.P., Friedl, R.R., Barker, J.R., Golden, D.M., Kurylo, M.J., Wine, P.H., Abbatt, J.P.D., Burkholder, J.B., Kolb, C.E., Moortgat, G.K., Huie, R.E., Orkin, V.L., 2011. Chemical Kinetics and Photochemical Data for Use in Atmospheric Studies. Evaluation no. 17, JPL Publication 10-6.
- Schwartz, S.E., 1986. Mass-transport considerations pertinent to aqueous phase reactions of gases in liquid-water clouds. In: Jaeschke, W. (Ed.), Chemistry of Multiphase Atmospheric Systems, NATO ASI Series, vol. G6, pp. 415–471.
- Seinfeld, J.H., Pandis, S.N., 1998. Atmospheric Chemistry and Physics: from Air Pollution to Climate Change. Wiley-Interscience, New York.
- Simpson, W.R., von Glasow, R., Riedel, K., Anderson, P., Ariya, P., Bottenheim, J., Burrows, J., Carpenter, L., Frieß, U., Goodsite, M.E., Heard, D., Hutterli, M.,

- Jacobi, H.-W., Kaleschke, L., Neff, B., Plane, J., Platt, U., Richter, A., Roscoe, H., Sander, R., Shepson, P., Sodeau, J., Steffen, A., Wagner, T., Wolff, E., 2007. Halogens and their role in polar boundary-layer ozone depletion. Atmospheric Chemistry and Physics Discussions 7, 4285—4403.
- Sjostedt, S.J., Abbatt, J.P.D., 2008. Release of gas-phase halogens from sodium halide substrates: heterogeneous oxidation of frozen solutions and desiccated salts by hydroxyl radicals. Environmental Research Letters 3, 045007.
- Smoydzin, L., von Glasow, R., 2009. Modelling chemistry over the Dead Sea: bromine and ozone chemistry. Atmospheric Chemistry and Physics 9. 5057–5072.
- Sommariva, R., von Glasow, R., 2012. Multiphase halogen chemistry in the tropical Atlantic Ocean. Environmental Science & Technology 46, 10429–10437.
- Spicer, C.W., Plastridge, R.A., Foster, K.L., Finlayson-Pitts, B.J., Bottenheim, J.W., Grannas, A.M., Shepson, P.B., 2002. Molecular halogens before and during ozone depletion events in the Arctic at polar sunrise: concentrations and sources. Atmospheric Environment 36, 2721–2731.
- Sridharan, U.C., Qiu, L.X., Kaufman, F., 1984. Rate constant of the OH \pm HO $_2$ reaction from 252 to 420 K. Journal of Physical Chemistry 88, 1281–1282.
- Stutz, J., Platt, U., 1996. Numerical analysis and estimation of the statistical error of differential optical absorption spectroscopy measurements with least-squares methods. Applied Optics 30, 6041–6053.
- Stutz, J., Ackermann, R., Fast, J.D., Barrie, L., 2002. Atmospheric reactive chlorine and bromine at the Great Salt Lake, Utah. Geophysical Research Letters 29, 18-1-18-4.
- Tans, P., Keeling, R., 2011. Trends in Atmospheric Carbon Dioxide. NOAA. http://www.esrl.noaa.gov/gmd/ccgg/trends.
- Tarasick, D.W., Bottenheim, J., 2002. Surface ozone depletion episodes in the Arctic and Antarctica from historical ozonesonde records. Atmospheric Chemistry and Physics 2, 197–205.
- Tas, E., Peleg, M., Pedersen, D.U., Matveev, V., Biazar, A.P., Luria, M., 2006. Measurement-based modeling of bromine chemistry in the boundary layer: 1. Bromine chemistry at the Dead Sea. Atmospheric Chemistry and Physics 6, 5589–5604.
- Thomas, J.L., Jimenez-Aranda, A., Finlayson-Pitts, B.J., Dabdub, D., 2006. Gas-phase molecular halogen formation from NaCl and NaBr aerosols: when are interface reactions important? Journal of Physical Chemistry A 110, 1859–1867, 2007, Erratum, 111, 7243–7244.
- Vogt, R., Crutzen, P.J., Sander, R., 1996. A mechanism for halogen release from seasalt aerosol in the remote marine boundary layer. Nature 383, 327–330.
- Vogt, R., Sander, R., von Glasow, R., Crutzen, P.J., 1999. Iodine chemistry and its role in halogen activation and ozone loss in the marine boundary layer: a model study. Journal of Atmospheric Chemistry 32, 375–395.
- von Glasow, R., Sander, R., 2001. Variation of sea salt aerosol pH with relative humidity. Geophysical Research Letters 28, 247–250.
- von Glasow, R., Sander, R., Bott, A., Crutzen, P.J., 2002. Modeling halogen chemistry in the marine boundary layer. 1. Cloud-free MBL. Journal of Geophysical Research 107, 4341.
- von Glasow, R., Crutzen, P.J., 2004. Model study of multiphase DMS oxidation with a focus on halogens. Atmospheric Chemistry and Physics 4, 589–608.
- von Glasow, R., 2006. Importance of the surface reaction OH+Cl on sea salt aerosol for the chemistry of the marine boundary layer a model study. Atmospheric Chemistry and Physics 6, 3571–3581.
- White, J.U., 1942. Long optical paths of large aperture. Journal of the Optical Society of America 32, 285–288.
- Zehavi, D., Rabani, J., 1972. Oxidation of aqueous bromide ions by hydroxyl radicals pulse radiolytic investigation. Journal of Physical Chemistry 76, 312—319.